

# How dilute are dilute solutions in extensional flows?

C. Clasen,<sup>a)</sup> J. P. Plog, and W.-M. Kulicke

*Institute of Technical and Macromolecular Chemistry, University of Hamburg,  
Germany*

M. Owens,<sup>b)</sup> C. Macosko, and L. E. Scriven

*Department of Chemical Engineering and Material Science, University of  
Minnesota, Minnesota*

M. Verani and G. H. McKinley

*Hatsopoulos Microfluids Laboratory, Massachusetts Institute of Technology,  
Cambridge, Massachusetts*

(Received 15 March 2006; final revision received 16 June 2006)

## Synopsis

We investigate the concentration dependence of the characteristic relaxation time of dilute polymer solutions in transient uniaxial elongational flow. A series of monodisperse polystyrene solutions of five different molecular weights ( $1.8 \times 10^6 \leq M \leq 8.3 \times 10^6$  g/mol) with concentrations spanning five orders of magnitude were dissolved in two solvents of differing solvent quality (diethylphthalate and oligomeric styrene). Optical measurements with a capillary breakup extensional rheometer of the rate of filament thinning and the time to breakup in each fluid are used to determine the characteristic relaxation time. A criterion for a lower sensitivity limit is introduced, in the form of a minimum concentration  $c_{\min}$  necessary for experimental resolution of the effects of polymeric viscoelasticity. This criterion is validated by experiment and comparison to numerical calculations with a multimode bead-spring dumbbell model. These calculations also rationalize previous paradoxical observations of extensional thinning in fluid threads of ultradilute polymer solutions in which stress relaxation apparently occurred faster than predicted by the Zimm theory. Above this minimum sensitivity limit we show that the effective relaxation time of moderately dilute solutions ( $0.01 \leq c/c^* \leq 1$ ) in transient extensional flow rises substantially above the fitted value of the relaxation time extracted from small amplitude oscillatory shear flow and above the Zimm relaxation time computed from kinetic theory and intrinsic viscosity measurements. This effective relaxation time exhibits a power-law scaling with the reduced concentration ( $c/c^*$ ) and the magnitude of the exponent varies with the thermodynamic quality of the solvent. The scaling of this “self-concentration” effect appears to be roughly consistent to that predicted when the dynamics of the partially elongated and overlapping polymer chains are described within the framework of blob theories for semi-dilute solutions. © 2006 The Society of Rheology. [DOI: 10.1122/1.2357595]

---

<sup>a)</sup>Present address: Department Chemische Ingenieurstechnieken, Katholieke Universiteit Leuven, Belgium; electronic mail: Christian.Clasen@cit.kuleuven.be

<sup>b)</sup>Present address: Drug Coating Process Developments, Boston Scientific, Maple Grove, Minnesota.

## I. INTRODUCTION

The critical overlap concentration of polymer coils, denoted  $c^*$ , is one of the most important characteristic values of a polymer solution. It is generally accepted that at concentrations  $c/c^* < O(1)$  the steric and frictional interactions of neighboring polymer coils are negligible and the rheological response of the fluid is solely governed by the sum of the deformation and hydrodynamic interactions of the isolated polymer coils and solvent which comprise the polymer solution. When these conditions exist, the theoretical description of a dilute solution given by the Rouse/Zimm theory is expected to be valid. At higher concentrations the solution becomes semidilute and eventually entangled depending on the degree of overlap of adjacent coils and their molar mass.

Graessley (1980) provides a simple definition of  $c^*$  that is widely accepted for demarcating the boundary separating the physical and rheological definition of dilute and semidilute polymer solutions

$$c^* = \frac{0.77}{[\eta]}, \quad (1)$$

where  $[\eta]$  is the intrinsic viscosity of the polymer solution which depends on the molar mass of the chain according to the Mark–Houwink–Sakurada equation  $[\eta] = K_{[\eta]} M^a$ , where  $K_{[\eta]}$  is a constant and the power-law index  $0.5 \leq a \leq 0.8$  varies with the quality of the solvent.

However, the definition of diluteness in Eq. (1) is only applicable for polymer coils that are not deformed greatly beyond their equilibrium configuration [for example in small amplitude oscillatory shear (SAOS) flow]. In extensionally-dominated flow fields, at conditions which satisfy the coil-stretch transition ( $\dot{\epsilon}\tau = 1/2$ ) a polymer coil becomes highly extended, leading to an increased interaction volume within which the chains may overlap, as reported by Dunlap and Leal (1987). Consequently polymer-polymer interactions are possible even at concentrations  $c/c^* < O(1)$ . The improper use of a near-equilibrium definition to characterize dynamic changes in conformation and the associated rheological responses to deformation has led to the recent introduction of the term “ultradilute” solution and a concentration of ultradilution,  $c^\infty$ , below which polymer solutions remain truly dilute even when the polymer chains are deformed well beyond their equilibrium state [Harrison *et al.* (1998)].

Characterization of the rheological properties of dilute and ultradilute solutions has rarely been carried out in extensional flows, because the extensional rheometry of polymer solutions has proven to be an experimental challenge far more complex than performing rheological measurements in a steady or dynamic shear flow. The challenge in characterizing extensional flows is to create and not disturb a homogeneous flow field while employing a liquid whose rheological properties are simple enough that they can be compared with theory. Consequently, new methods for the quantitative study of dilute polymer solutions in extensional flows are desired. Recent developments in non-invasive experimental methods for characterizing extensional flow fields are reviewed in the monograph by Nguyen and Kausch (1999).

The first mechanical studies of the state of stress for polymer solutions in a well-defined uniaxial flow field were made by Sridhar *et al.* [Matta and Tytus (1990); Sridhar *et al.* (1991)] using the filament stretching device. A comparison of different approaches for realizing this type of experiment [Anna *et al.* (2001)] showed for the first time the possibility of quantitative determination of the transient extensional viscosity for well-characterized dilute solutions in a purely uniaxial flow field. A recent overview of filament stretching rheometry is given in [McKinley and Sridhar (2002)]. Filament stretching

instruments are complex and expensive and, furthermore, reliable experiments are very difficult for low viscosity fluids with zero shear-rate viscosities less than  $\sim 0.5$  Pa s due to inertial and gravitational effects [McKinley and Sridhar (2002)]. Recent studies of jet breakup [Christanti and Walker (2001)] and drop pinch-off [Amarouchene *et al.* (2001); Cooper-White *et al.* (2002)] as well as the groundbreaking work of Entov and co-workers [Entov *et al.* (1988); Bazilevskii *et al.* (1990, 1997); Entov and Hinch (1997)] have demonstrated the efficacy of capillarity-driven thinning flows for the determination of transient extensional material functions. Capillary-thinning devices have been developed recently by a number of laboratories [Liang and Mackley (1994); Kolte and Szabo (1999); McKinley and Tripathi (2000); Stelter and Brenn (2000); Anna and McKinley (2001); Bazilevskii *et al.* (2001); Stelter *et al.* (2002)] and the dynamics of the elastocapillary thinning process are reviewed in McKinley (2005).

It is important to note the distinctions between the dynamics of capillary thinning and those of filament stretching rheometry for dilute polymer solutions. For example, Gupta *et al.* (2000) investigated the effects of varying the concentration and molar mass of dilute and semidilute polystyrene solutions on the extensional stress growth in filament stretching experiments. In order to ensure elastic stresses were large enough to be measured accurately and in order to overcome gravitational effects, they had to perform the tests at large extension rates  $\dot{\epsilon}$ , corresponding to Weissenberg numbers  $Wi = \tau_0 \dot{\epsilon} \gg 1$  where  $\tau_0$  is the longest relaxation time of the polymer solution. In this limit, the chain deformation becomes increasingly affine, and Brownian dynamics simulations and experiments both show that the measured curves of the transient extensional viscosity begin to superpose and approach a single limiting curve as a function of strain [Larson (2005)]. It is thus very difficult to probe directly the effects of concentration changes on the longest relaxation time of the solution. By contrast, the theoretical analysis by Entov and Hinch (1997), in conjunction with supporting experimental data [Anna and McKinley (2001)], shows that the elastocapillary balance achieved in capillary-thinning experiments results in a natural stretching rate of  $\dot{\epsilon} = 2/(3\tau_0)$  or, equivalently, a Weissenberg number  $Wi = \tau_0 \dot{\epsilon} = 2/3$ . This self-selected value is just sufficiently above the critical value of 0.5 (corresponding to the coil-stretch transition) to keep the polymer chain stretching such that the growing elastic stress balances the increasing level of capillary pressure in the thinning cylindrical thread. All of the shorter relaxation modes in the chain experience the same elongation rate  $\dot{\epsilon}$ , corresponding to Weissenberg numbers below 0.5, and consequently their contributions to the material response decay. The dynamics of elastocapillary thinning are therefore controlled directly by the longest relaxation process which corresponds to the relaxation-controlled unraveling of the entire chain. Capillary thinning and break-up experiments thus provide a convenient means for probing chain-chain interactions as a function of polymer concentration through measurements of the characteristic time scale of the solution in a strong extensional flow.

Several investigations of transient elongational behaviour have been reported for a range of different polymers and molar masses [Liang and Mackley (1994); Bazilevskii *et al.* (1997); Stelter and Brenn (2000); Anna and McKinley (2001); Anna *et al.* (2001)] in semidilute to dilute solutions. Recently Bazilevskii *et al.* (2001), Stelter *et al.* (2002) and Tirtaatmadja *et al.* (2006) have studied flexible polymers in dilute and ultradilute solution, finding that the characteristic relaxation time extracted from capillary-thinning or jet-thinning experiments continues to depend strongly on the concentration even below the critical overlap concentration  $c^*$ , in contrast to expectations of the Rouse/Zimm theory. In addition, Bazilevskii *et al.* and Tirtaatmadja *et al.* observed a power-law dependency of the relaxation time on the concentration. Similar power-law variations of the rheological properties for apparently dilute aqueous polymer solutions have also been

observed by Kalashnikov (1994) and by Tam and Tiu (1993). We also note that whereas Stelter *et al.*, Tirtaatmadja *et al.*, and Christanti and Walker (2001) all reported relaxation times that *exceeded* the expected relaxation time from the Zimm theory, Bazilevskii *et al.* (2001) also found that for very dilute solutions (down to concentrations as low as 0.2 ppm) the power-law scaling lead to relaxation times that fell *below* the predicted Zimm relaxation time.

In order to resolve this discrepancy, the present paper focuses on a detailed investigation of the capillary-thinning dynamics and breakup for dilute and ultradilute monodisperse polymer solutions. In order to quantitatively analyze the elastocapillary thinning process and extract the longest relaxation time for very dilute solutions it is first necessary to reconsider carefully the fluid dynamics of filament thinning, in particular to answer the question of how much of the tensile stress in the thinning thread is carried by the polymer and how much by the solvent. In other words, we seek to understand under what physical conditions a coil-stretch transition that occurs on the molecular scale can affect the resulting macroscopic fluid dynamics. This provides an effective distinction between a dilute and an ultradilute polymer solution for this particular flow configuration.

In this paper we present experimental investigations of capillary thinning using high molar masses and nearly monodisperse polystyrene samples ( $1.8 \leq M \leq 8.3 \times 10^6$  g/mol). The chains are dissolved in two different high and low viscosity solvents with qualities ranging from good (diethylphthalate) to near theta conditions (styrene oligomer) over a range of concentrations spanning five orders of magnitudes. We thus investigate the elongational response under semidilute, dilute, and ultradilute conditions. In addition, numerical calculations (using a multimode FENE-P formulation) of the transient stress evolution in the thinning filament are used to determine the relative contribution of the polymer chains to the overall stress balance as a function of concentration and molar mass. This enables us to determine the lower sensitivity limit of the capillary-thinning technique and to identify systematic discrepancies that can arise under very dilute conditions.

## II. EXPERIMENT AND ANALYSIS METHODS

### A. Sample preparation

The polystyrene samples were provided by Polysciences Inc., Warrington, PA, (sample A:  $M_w = 1.8 \times 10^6$  g/mol, and sample D:  $M_w = 6.0 \times 10^6$  g/mol), Polymer Laboratories, Amherst, MA (sample C:  $M_w = 5.7 \times 10^6$  g/mol and sample E:  $M_w = 8.3 \times 10^6$  g/mol), and also Polymer Standard Services, Ontario, NY (sample B:  $M_w = 2.8 \times 10^6$  g/mol). Molar mass  $M_w$  and polydispersity  $M_w/M_n$  were verified by size exclusion chromatography with a multiangle light scattering detector. Two different batches of oligomeric styrene with a degree of polymerization of  $\sim 5$  (Piccolastic A-5 Resin) as a solvent for Boger fluids were provided by Hercules, (Wilmington, DE). The diethylphthalate (DEP) solvent was supplied by Merck, (Darmstadt, Germany) and used as received.

The solutions of polystyrene in styrene oligomer (Boger fluids) were prepared in two different ways:

(a) Sample A (0.166 wt %), sample B (0.025 wt %), and sample D (0.107 wt %) were prepared by adding the polymer to the oligomer at room temperature and placing the samples in an oven at 100 °C, without stirring (samples A and D) and with repeated agitation (sample B), until the polymer dissolved over several weeks.

(b) Sample C (0.25 wt %) and sample E (0.1 wt %) were prepared by dissolving the

**TABLE I.** Physical parameters of the polystyrene solutions in the near-theta solvent styrene oligomer (Boger fluids).

Sample	$M_w/(g/mol)$	$M_w/M_n$	$[\eta]/(cm^3/g)$	$L$	$\eta_s/(Pa\ s)$	$\gamma/(N/m)$	$\rho/(kg/m^3)$	$\tau_z/(s)$
A	$1.80 \times 10^6$	1.02	63.7	73	33	0.0378	1026	0.64
B	$2.84 \times 10^6$	1.13	82.2	90	51	0.0378	1026	2.01
C	$5.67 \times 10^6$	1.09	121.1	126	40	0.0378	1026	4.64
D	$6.00 \times 10^6$	1.22	125.0	130	33	0.0378	1026	4.18
E	$8.27 \times 10^6$	1.13	150.0	151	40	0.0378	1026	8.35

polymer in minute amounts of toluene, mixing with the oligomer and continuous evaporation of the toluene at 10 Pa pressure under steady agitation of the sample at 50 °C over several weeks, controlling the evaporation process by weight.

The different concentrations used in the experiments were achieved by diluting the above samples with the respective batch of Piccolastic A-5.

Preparation of the polystyrene/DEP solutions involved dissolving the respective amount of polymer in the solvent. Homogenization was achieved by slow continuous agitation over a period of time not shorter than 7 days.

The relevant physical data of the solutions are compiled in Tables I and II. The intrinsic viscosities  $[\eta]$  of the polystyrene/diethylphthalate solutions were determined using a micro-Ubbelohde viscometer with a No. IIc capillary ( $\varnothing=0.95$  mm) (Schott-Geräte GmbH, Mainz, Germany). The intrinsic viscosities for the polystyrene in styrene oligomer solutions (Boger fluids) were calculated from the respective Mark–Houwink–Sakurada equation. The finite extensibility parameter  $L$  was calculated from molecular parameters as described in Sec. II D. The solvent viscosities  $\eta_s$  of the Boger fluids were determined from fitting Eqs. (2) and (3) to SAOS data. A noticeable difference in solvent viscosities between the first batch (used for samples A and D) and the second batch of styrene oligomer (used for samples B, C, and E) is observed. The slightly higher solvent viscosity of the solutions of sample B in comparison to solutions of samples C and E in the same batch of styrene oligomer is most likely attributable to inexorable aging and polymerization of the oligomeric solvent due to residual traces of initiator in the polymer and/or ultraviolet light during the longer preparation process of solutions of sample B. The solvent viscosity  $\eta_s$  of the diethylphthalate was measured in steady shear via cone and plate rheometry. Surface tensions  $\gamma$  were experimentally determined using a Krüss K10ST Tensiometer (Hamburg, Germany).

## B. Shear rheology

The rheology of the test fluids in both steady and dynamic shear flow was investigated using an AR1000 N rheometer as well as two Rheometric Series ARES (TA Instruments, Newcastle, DE) with cone and plate fixtures,  $\varnothing=40$  mm, cone angle=0.04 rad.

**TABLE II.** Physical parameters of the polystyrene solutions in the good solvent DEP.

$M_w/(g/mol)$	$M_w/M_n$	$[\eta]/(cm^3/g)$	$L$	$\eta_s/(Pa\ s)$	$\gamma/(N/m)$	$\rho/(kg/m^3)$	$\tau_z/(s)$
$8.27 \times 10^6$	1.13	601	95.0	0.011	0.0375	1118	0.0107
$5.67 \times 10^6$	1.09	464	81.1	0.011	0.0375	1118	0.0057
$2.84 \times 10^6$	1.13	283	59.9	0.011	0.0375	1118	0.0017

The longest relaxation time  $\tau_0$  (as measured by shear flow experiments) was obtained by fitting the predictions of the Rouse/Zimm model for dilute solutions to the measured linear viscoelastic moduli  $G'(\omega)$  and  $G''(\omega)$ . For Boger fluids with an oligomeric solvent, an additional weak elastic contribution of the solvent to the total measured loss and storage modulus must be included

$$G' = \frac{\eta_s \tau_s \omega^2}{1 + (\tau_s \omega)^2} + \frac{cRT}{M_w} \sum_{i=1}^{N_{\text{modes}}} \left[ \frac{(\tau_0 \omega)^2}{i^{4+2\tilde{\sigma}} + (\tau_0 \omega)^2} \right], \quad (2)$$

$$G'' = \frac{\eta_s \omega}{1 + (\tau_s \omega)^2} + \frac{cRT}{M_w} \sum_{i=1}^{N_{\text{modes}}} \left[ \frac{(\tau_0 \omega) i^{2+\tilde{\sigma}}}{i^{4+2\tilde{\sigma}} + (\tau_0 \omega)^2} \right], \quad (3)$$

where  $R=8.314$  J/mol K is the universal gas constant,  $\omega$  is the angular frequency,  $T$  is the absolute temperature, and  $\tau_s$  is the relaxation time of the oligomeric solvent [Mackay and Boger (1987)]. The longest relaxation time  $\tau_0$  is connected to the Zimm spectrum  $\tau_i$  with a number of modes  $N_{\text{modes}}$  by a recursion relationship

$$\tau_i = \frac{\tau_0}{i^{2+\tilde{\sigma}}} \quad \text{for } i = 1, 2, \dots, N_{\text{modes}}, \quad (4)$$

where  $\tilde{\sigma}$  is a measure of the hydrodynamic interaction between the segments of the polymer chain and the surrounding solvent. This parameter can be related to the hydrodynamic interaction parameter  $h^*$  of the Zimm model via a correlation originally published by Thurston [Bird *et al.* (1987)]

$$\tilde{\sigma} = -1.40(h^*)^{0.78}. \quad (5)$$

For negligible hydrodynamic interactions ( $h^*=0$ ) the Rouse spectrum is obtained; for dominant hydrodynamic interactions, as in the case of Boger fluids, the parameter  $h^*$  approaches a limiting value of 0.25, resulting in the Zimm scaling of  $2+\tilde{\sigma} \approx 1.5$ . For polystyrene in the relatively good solvent DEP an excluded volume exponent  $\nu=0.567$ , determined from viscometric measurements of the intrinsic viscosities for the different molar masses, gives  $h^*=0.14$  when applying the approximation  $3\nu=2+\tilde{\sigma}$ . This value is in good agreement for example with  $h^*=0.15$  for polystyrene in the good solvent aroclor as reported by Amelar *et al.* (1991).

The number of modes can be varied depending on the desired resolution of the viscoelastic spectrum. The Hookean dumbbell corresponds to  $N_{\text{modes}}=1$ . Amelar *et al.* (1991) suggest that the appropriate molecular mass associated with a single spring should be in the range 5000–10 000 g/mol for polystyrene, resulting in values for the samples in this report of  $N_{\text{modes}}=240$ –1100. In practice due to the rapid decay of higher modes and the limited range of frequencies used, a smaller number of modes of  $8 < N_{\text{modes}} < 15$  is sufficient for the determination of  $\tau_0$  and computation of the linear viscoelastic properties.

### C. Capillary thinning experiments

The capillary thinning experiments reported here were carried out using (i) a CaBER version1 (Thermo Electron, Karlsruhe, Germany) using circular endplates with a diameter  $D_p=6$  mm, and (ii) a self-built apparatus with endplates of diameter  $D_p=3$  mm. In each case an approximately cylindrical liquid bridge of height  $h_0$  was formed between the two endplates. Both setups employed a step strain to separate the plates from their initial distance  $h_0$ , reaching their final separation  $h_f$  in 50 ms. The midplane diameter evolution



was followed using a laser micrometer (CaBER) or a Cohu charge coupled device (CCD) camera recording at 30 frames/s (self-built apparatus). The aspect ratio increases from an initial value  $\Lambda_0=h_0/D_p$  to a final aspect ratio  $\Lambda_f=h_f/D_p$ . In the present experiments we use  $\Lambda_0=0.5$  and  $\Lambda_f=1.3$  (CaBER) or  $\Lambda_0=1.0$  and  $\Lambda_f=2.5$  (self-built apparatus) to minimize the perturbative effects of gravitational forces and fluid inertia [Slobozhanin and Perales (1993)] and thus to keep the height  $h_0$  of the fluid sample on the order of or below the capillary length  $l_{\text{cap}}$ ,

$$h_0 \leq l_{\text{cap}} = \sqrt{\frac{\gamma}{\rho g}} \quad (6)$$

with the surface tension  $\gamma$  and the fluid density  $\rho$ . For further details on the geometry and aspect ratios see Rodd *et al.* (2005).

#### D. Numerical calculations of elastocapillary thinning

For numerical calculations of the transient evolution in the filament diameter  $D(t)$  we follow the approach of Entov and Hinch (1997). The governing stress balance in a thinning viscoelastic filament, consisting of the product of the solvent viscosity  $\eta_s$  times the extension rate  $\dot{\epsilon}$ , the axial tensile force  $F_z$ , the tensile stress difference arising from the dissolved polymer  $\Delta\sigma_p$ , the surface tension  $\gamma$ , and gravitational forces [Eggers (1997)], is given by

$$3\eta_s\dot{\epsilon} = \frac{4F_z(t)}{\pi D(t)^2} - \Delta\sigma_p - \frac{2\gamma}{D(t)} + \frac{\rho g D_0^2 h_0}{D(t)^2}. \quad (7)$$

This expression can be simplified by noting that, once the gravitational forces are overcome by the symmetric axial flow induced by capillarity in the necked region, the last term on the right hand side can be neglected [Kolte and Szabo (1999); McKinley and Tripathi (2000)]. The numerically calculated evolution of the midfilament diameter  $D(t)$  can thus be compared quantitatively with experimental measurements below a critical diameter  $D \leq 0.5l_{\text{cap}}$ . For our systems this constraint corresponds to filament diameters less than  $D \leq 1$  mm. The evolution of a self-thinning bridge is described by a self-similar solution and the evolution of the tensile force  $F_z(t)$  can thus be related to the rate of change in the diameter  $D(t)$ . McKinley and Tripathi (2000) showed that the coefficient of proportionality

$$X = \frac{F_z(t)}{\pi\gamma D(t)} \quad (8)$$

for the typical experimental conditions in a capillary thinning of a Newtonian liquid is given by  $X=0.7127$  as determined by Papageorgiu (1995) for self-similar capillary pinch off of a viscous fluid. However, as the contribution of the elastic stresses becomes large in comparison to the viscous stresses the filament becomes increasingly cylindrical and the correction factor  $X$  is predicted to approach unity [Entov and Hinch (1997)].

Using Eq. (8), the force balance reduces to the following “purely local” or “zero-dimensional” formulation incorporating the viscous stress of the solvent  $3\eta_s\dot{\epsilon}$ , the capillary pressure  $2\gamma/D$  and the additional tensile stress  $\Delta\sigma_p$  from the polymer

$$3\eta_s\dot{\epsilon} = (2X - 1)\frac{2\gamma}{D} - \Delta\sigma_p. \quad (9)$$

The polymer contribution  $\Delta\sigma_p$  is taken here to correspond to a multimode FENE dumbbell model

$$\Delta\sigma_p(t) = \sigma_{p,zz} - \sigma_{p,rr} = \sum_i^{N_{\text{modes}}} G_i f_i (A_{zz,i} - A_{rr,i}). \quad (10)$$

The tensor  $\mathbf{A}$  is the ensemble average second moment configuration tensor

$$\mathbf{A} = \sum_{i=1}^{N_{\text{modes}}} \mathbf{A}_i = \frac{\langle \mathbf{Q}\mathbf{Q} \rangle}{Q_{\text{eq}}^2/3} \quad (11)$$

of the entire chain normalized with the equilibrium coil size  $Q_{\text{eq}}^2$ . In the Rouse-Zimm theory the contribution  $G_i$  to the elastic modulus of each mode is invariant with mode number and is only a function of the number density of polymer chains in solution [Ferry (1980)]:

$$G = nk_B T = \frac{cRT}{M_w}. \quad (12)$$

The evolution equations for the  $i$ th mode of  $\mathbf{A}$ , using a multimode FENE-P mode algorithm, are given by

$$\overset{\nabla}{\mathbf{A}}_i = -\frac{1}{\tau_i} (f_i \mathbf{A}_i - \mathbf{I}) \quad (\text{for } i = 1, 2, \dots, N_{\text{modes}}), \quad (13)$$

where  $\overset{\nabla}{\mathbf{A}}_i$  is the upper convected derivative  $\overset{\nabla}{\mathbf{A}}_i = \dot{\mathbf{A}}_i - \nabla \mathbf{v}^T \cdot \mathbf{A}_i - \mathbf{A}_i \cdot \nabla \mathbf{v}$  with  $\dot{\mathbf{A}}_i$  denoting the substantial time derivative and  $\nabla \mathbf{v}^T$  the velocity gradient tensor [Bird *et al.* (1987)].

The finite extensibility factor  $f_i$  for each mode is connected to the finite extensibility parameter  $L^2$  for the entire polymer chain by the expressions

$$f_i = \frac{1}{1 - \frac{\text{tr} \mathbf{A}_i}{L_i^2}}, \quad (14)$$

$$L_i^2 = \frac{L^2}{i^{2\nu}}. \quad (15)$$

The finite extensibility parameter  $L^2$  for the entire chain can be fully described in terms of molecular parameters such as the C–C bond angle  $\theta$  and the number of bonds  $j$  of a monomer unit with molar mass  $M_u$ , the characteristic ratio  $C_\infty$  for a given polymer and the excluded volume exponent  $\nu$ :

$$L^2 = 3 \left[ \frac{j(\sin \theta/2)^2 M_w}{C_\infty M_u} \right]^{2(1-\nu)}. \quad (16)$$

The axial and radial deformation components of the constitutive model of Eq. (13) satisfy the equations

$$\dot{A}_{zz,i} - 2\dot{\epsilon} A_{zz,i} = -\frac{1}{\tau_i} (f_i A_{zz,i} - 1), \quad (17)$$

$$\dot{A}_{rr,i} + \dot{\epsilon} A_{rr,i} = -\frac{1}{\tau_i} (f_i A_{rr,i} - 1). \quad (18)$$



The time-varying deformation rate  $\dot{\epsilon}$  in a capillary thinning experiment can be expressed in terms of the rate of necking of the diameter  $D$  through the continuity equation by equating the local velocity gradients at the mid-plane in the axial and radial directions, leading to

$$\dot{\epsilon} = \frac{-2}{D} \dot{D}. \quad (19)$$

This expression, when combined with the force balance from Eq. (9) and the definition of elastic stress in Eq. (10), defines the overall stress balance

$$(2X - 1) \frac{2\gamma}{D} = 3\eta_s \dot{\epsilon} + \frac{cRT}{M_w} \sum_{i=1}^{N_{\text{modes}}} f_i(A_{zz,i} - A_{rr,i}). \quad (20)$$

Equations (17)–(20) form a coupled set of ordinary differential equations that can be solved numerically to describe the temporal evolution of the midfilament diameter during capillary thinning. Input parameters are given by the independently measured physical parameters of the polymer chain and the solution (molar mass  $M_w$ , finite extensibility  $L^2$ , surface tension  $\gamma$ , density  $\rho$ , solution viscosity  $\eta_0$ , and solvent viscosity  $\eta_s$ ) and the initial state of the filament after cessation of the sudden extension (initial diameter  $D_0$  and initial conformation  $A_{zz,i}^0$ ).

We set  $N_{\text{modes}}=8$  for the following calculations. The (low) number of modes chosen here is justifiable by noting that during the period when elastic stresses dominate filament thinning the self-selected Weissenberg number for the flow is  $Wi = \tau_0 \dot{\epsilon} = 2/3$ , and is determined by the longest mode [Entov and Hinch (1997)]. All other modes  $N_i$  for  $i > 1$  are in a relaxed state since their respective Weissenberg numbers [given by Eq. (4)] are below 0.5 until very near the end of the stretching process. These modes therefore do not contribute significantly to the total stress.

The unknown initial conformation and the initial stretch of the polymer after the step strain can be estimated according to the procedure proposed by Anna and McKinley (2001). We assume that all three terms in Eq. (9) initially balance each other during the rearrangement of the fluid column at the cessation of the initial stretch. By replacing  $\dot{\epsilon} = 2/(3\tau_0)$  in the viscous contribution we obtain

$$\frac{2\gamma}{D_0} - \frac{2\eta_s}{\tau_0} = \frac{cRT}{M_w} \sum_{i=1}^{N_{\text{modes}}} A_{zz,i}^0. \quad (21)$$

For the numerical calculations we assume an even distribution of the initial deformation over all modes; however, the numerical solutions were not sensitive to the choice of this initial deformation.

The parameter  $X$  in Eqs. (8) and (20) is not constant over time. As the contribution of the elastic stresses becomes large in comparison to the viscous stresses the filament becomes increasingly cylindrical and the factor  $X$  should approach unity. A self-consistent determination of the axial force in the filament  $F_Z(t)$  requires a full one- or two-dimensional numerical analysis of the thinning dynamics [Yao *et al.* (2000); Clasen *et al.* (2006)] which is beyond the scope of the present study. The effect of varying  $X$  is rather small; however, for consistency in the numerical calculations, we retain the factor  $X$  for very low polymer concentrations in order to describe accurately the initial part of the Newtonian flow region. We adjust  $X$  and vary the value from 0.7127 for the pure solvent ( $c \rightarrow 0$ ) to unity for polymer solutions which show a clear onset of polymeric effects in the necking process.

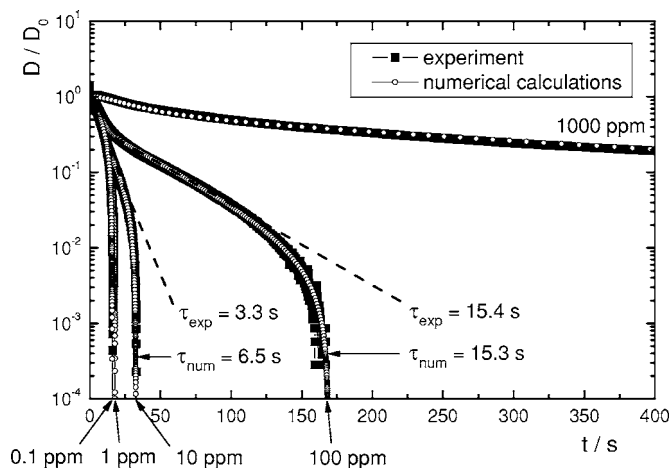


**FIG. 1.** Comparison of the numerically calculated evolution in the filament diameter (open symbols) with experimental data from capillary thinning experiments (closed symbols) for a dilution series of the Boger fluid from sample E ( $M_w = 8.3 \times 10^6$  g/mol) for different concentrations spanning  $0.1 \leq c \leq 1000$  ppm. In addition the relaxation times  $\tau_{\text{exp}}$ , determined from fitting the elasto-capillary thinning regime [Eq. (22)] of the experiments, and  $\tau_{\text{num}}$ , determined from fitting the numerical calculations [Eqs. (17)–(21)] to the experimental data, are given for selected concentrations.

An example of the agreement between experimental measurements of the diameter evolution and the corresponding numerical calculations is shown in Fig. 1 for a dilution series of the Boger fluid from sample E ( $M_w = 8.3 \times 10^6$  g/mol), with the concentration spanning five orders of magnitude. Similar levels of agreement are obtained for each dilution series, and we now proceed to examine how to analyze experimental measurements of filament profiles.

### E. Determination of relaxation times from elastocapillary regime

Although we have just demonstrated above how it is possible to determine the longest relaxation time  $\tau_0$  by fitting the entire capillary thinning data, usually a simpler analysis is employed. As noted by Entov and Hinch (1997) for a viscoelastic polymer solution in which the chains become highly stretched, Eq. (9) offers the possibility of an *elastocapillary* balance. The viscous stress of the solvent is negligibly small and the filament becomes a cylindrical thread ( $X=1$ ). Provided finite extensibility effects are not important ( $L^2 \rightarrow \infty$ ), the decay rate in the measured diameter depends only on the longest relaxation time and is given by [Entov and Hinch (1997); Clasen *et al.* (2006)]:

$$\frac{D(t)}{D_0} = \left( \frac{GD_0}{4\gamma} \right)^{1/3} \exp(-t/3\tau_0). \quad (22)$$

The additional factor of  $2^{-1/3}$  in the prefactor of Eq. (22), obtained from a complete one-dimensional self-similar analysis is missing in the original theory due to a simplifying approximation in the zero-dimensional theory [Clasen *et al.* (2006)], though this does not change the exponential decay rate. The longest relaxation time  $\tau_0$  of the polymers undergoing molecular relaxation-controlled unraveling in the thinning filament can be easily obtained from this relationship by determining the slope of the linear regime in a semilog plot as shown in Fig. 1 by the dashed lines. The validity of this approach and its consistency with other methods has been reported in several publications for a range of

different polymers, molar masses and concentrations in dilute to semidilute solutions [Liang and Mackley (1994); Bazilevskii *et al.* (1997); Stelter and Brenn (2000); Anna and McKinley (2001); Anna *et al.* (2001); Bazilevskii *et al.* (2001); Stelter *et al.* (2002); Plog *et al.* (2005)]. In all of these cases, provided there is a *sufficiently large polymer concentration*, an elastocapillary balance holds for a long enough period that the exponential decay of the filament can be observed and the data regressed to Eq. (22).

However, as we show in detail later, the more dilute a solution becomes, the harder it becomes to detect a distinct regime of purely exponential thinning. This is because the initial Newtonian flow and the finite extensibility of the polymer chains cannot be neglected during the short intermediate regime of exponential thinning. Nevertheless, linear fits of experimental data on a semilog-plot to Eq. (22) are often performed even for very dilute solutions to extract a relaxation time and initially we will follow this procedure.

The numerical calculations described in Sec. II D result in predicted profiles for the growth in the elastic stress and the decay rate of the filament diameter. The latter expression can be compared directly with the experimental observations. In cases for which the exponential decay of the filament could be observed over sufficiently long periods of time, the longest relaxation time  $\tau_0$  determined from reliable regressions of Eq. (22) to experimental data and the relaxation time used in numerical calculations coincide as can be seen for example in Fig. 1 for a concentration of 100 ppm. However, for very low polymer concentrations the numerically predicted profile, calculated using the apparent relaxation time obtained from regressing the data in the very brief period of exponential thinning, does not match the experimentally observed evolution in the filament diameter. In these cases we use  $\tau_0$  as an *adjustable* parameter to fit the experiments with the numerical calculations and thus determine the governing relaxation time  $\tau_0$  for filament thinning. This discrepancy between an apparent longest relaxation time, determined from experimental data in the elastocapillary thinning regime according to Eq. (22) (dashed line), and the longest relaxation time determined by fitting the numerical calculations can be observed in Fig. 1 for a concentration of 10 ppm. In Sec. III we will compare  $\tau_0$  as determined by Eq. (22) to the value obtained by fitting with numerical calculations and provide a criterion for conditions under which Eq. (22) may be safely used.

### III. RESULTS AND DISCUSSION

#### A. Capillary thinning

We first present our experimental measurements of capillary thinning in viscous oligomeric solvents and in the low viscosity DEP solvent. Figure 2 depicts the temporal evolution of the midplane diameter that can be determined experimentally. The figure shows three representative dilution series that demonstrate the critical characteristics of the thinning behaviour, the complete data set for all of the capillary thinning experiments can be found in the Appendix.

Figure 2(a) shows the filament evolution of Boger fluids determined by analyzing still frames captured by a CCD camera. It is evident that the diameter resolution of this method is lower than that of the laser micrometer shown in Fig. 2(b) for Boger fluids and in Fig. 2(c) for diethylphthalate solutions. However, determination of the exponential decay of the diameter with time according to Eq. (22) is still possible using Fig. 2(a) because the onset of finite extensibility effects occurs below the resolution limit of the imaging system.

It can clearly be seen from Figs. 2(a) and 2(b), that at early times the necking behavior of all solutions follows the thinning behavior of the Newtonian solvent as expected from the analysis of Entov and Hinch (1997). The necking is controlled by a *viscocapillary*

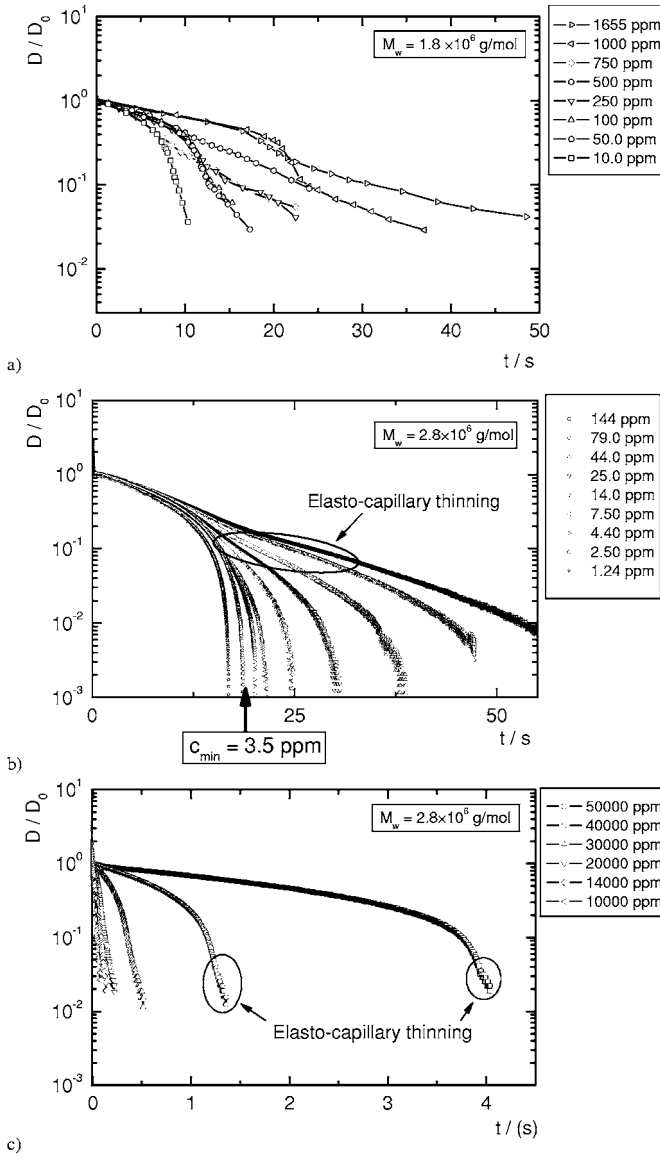


**FIG. 2.** Reduced diameter  $D/D_0$  as a function of time  $t$  in capillary thinning experiments for several dilution series of narrowly distributed polystyrene samples. The samples are dissolved respectively in (a) styrene oligomer (Boger fluids), profiles determined from CCD camera video images of the thinning filament; (b) styrene oligomer, profiles determined with a laser micrometer. In addition to the experimental data Fig. 2(b) also shows the theoretical critical concentrations  $c_{min}$  calculated from Eq. (41) that depicts the minimum concentration for an observable influence of polymer on the capillary thinning behavior.

balance of the viscous stress  $3\eta_s\dot{\epsilon}$  in the force balance of Eq. (9) and the capillary pressure. In this regime the diameter varies linearly in time

$$D(t) = D_0 - \frac{(2X - 1)\gamma}{3\eta_s}t \tag{23}$$

and the extension rate in the necking filament, given by

$$\dot{\varepsilon}(t) = \frac{2(2X-1)\gamma}{3\eta_s} \frac{1}{D(t)} \quad (24)$$

slowly climbs.

The polymeric stress associated with the initial conformation  $A_{zz,i}^0$  [Eq. (21)], that is caused by the step strain, decays rapidly during the early stages of thinning since the extension rate is insufficient to keep even the longest mode excited. However, as thinning progresses the extension rate rises, the polymer coils become extended, and the system crosses over to a second phase of *elastocapillary* thinning. In this regime the filament thins exponentially according to Eq. (22). It is clear from Fig. 2(b) that this crossover shifts to earlier times and higher values of  $D(t)/D_0$  as the polymer concentration is raised. Finally, at late times, the finite extensibility limit of the unraveling polymer is approached and the FENE factor  $f_i$  [Eq. (14)] in the force balance for the filament can no longer be neglected and the thinning behavior deviates from the exponential regime of elastocapillary thinning. In this third phase the decay rate becomes linear again corresponding to a viscous liquid with a very high and anisotropic elongational viscosity resulting from the fully extended polymer chains. The filament diameter evolves according to

$$D(t) = \frac{\gamma}{\eta_E} (t_{br} - t), \quad (25)$$

with  $t_{br}$  the breakup time and  $\eta_E$  the steady uniaxial elongational viscosity.

This third phase is not observed for the diethylphthalate solutions in Fig. 2(c) because the filament diameter drops below the resolution limit of the experiment before the effects of finite extensibility are observed. The initial phase of viscopillary thinning in Fig. 2(c) also shows a strong concentration dependence at higher concentrations. This is because the viscous resistance to thinning is determined by the viscosity of the total entangled solution rather than by the pure solvent as is the case for dilute or semi-dilute Boger fluids shown in Fig. 2(b).

The relaxation times  $\tau_0$  determined by fitting data from the intermediate elastocapillary phase in Figs. 2 and 14 to Eq. (22) are shown in Fig. 3. The relaxation times show a strong dependence on the concentration and decrease monotonically with decreasing concentration. To understand the molar mass dependence, one has to keep in mind that the styrene oligomers used as solvents in this report had different viscosities (Table I). Kinetic theory shows that the longest relaxation time of an isolated polymer coil in dilute solution is proportional to the solvent viscosity

$$\tau_0 = \frac{1}{U_{\eta r}} \frac{\eta_p}{G} = \frac{1}{U_{\eta r}} \frac{[\eta] \eta_s M_w}{RT} \quad (26)$$

where  $U_{\eta r} = \tau_\eta / \tau_0$  is the universal ratio of the characteristic relaxation time  $\tau_\eta$  of a dilute polymer solution system and the longest relaxation time  $\tau_0$ . The numerical value of the universal ratio depends on the relaxation spectrum of the specific constitutive model [Öttinger (1996)] (with  $U_{\eta r} = 2.39$  for theta solvents to  $U_{\eta r} \sim 1.8$  for good solvents). From Eq. (26) it can be seen that for a homologous series of polystyrene solutions the slightly *higher* relaxation times of the Boger fluid with  $M_w = 5.7 \times 10^6$  g/mol in comparison to  $M_w = 6.0 \times 10^6$  g/mol are explained by the higher solvent viscosity of the styrene oligomer used in this set of fluids (see Table I).

In addition to the experimentally determined relaxation times, Fig. 3 depicts graphically (by broken lines) the expected variation in the critical overlap concentration  $c^*$  as

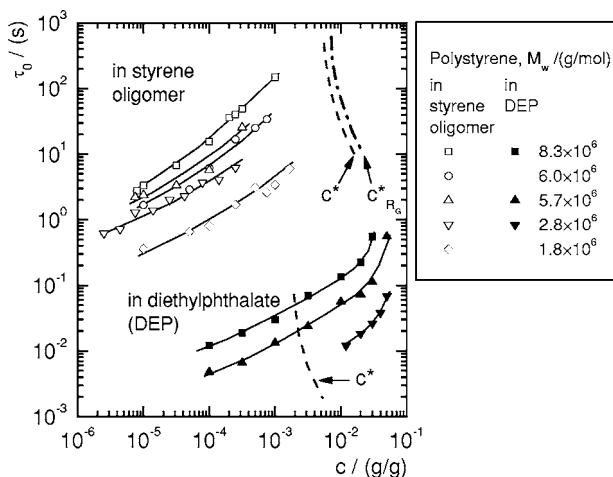


**FIG. 3.** Relaxation time  $\tau_0$  as a function of the concentration  $c$ , determined by regression of the experimental data in the exponential decaying regime of Figs. 2 and 14 to Eq. (22). The dashed lines map the variation of relaxation time  $\tau_0$  with critical concentrations  $c^*$ . These values were determined by extrapolating the observed trends of relaxation times to the critical values determined from Eqs. (1) and (27).

calculated from the molar mass dependence of the intrinsic viscosity [Eq. (1)]. These curves are obtained by extrapolating the observed trends of relaxation times to these respective concentrations. The intrinsic viscosity is typically measured using an Ubbelohde viscometer of appropriate bore size for the fluid of interest. The Mark–Houwink–Sakurada relation for polystyrene in DEP, which is a relatively good solvent at  $T = 25^\circ\text{C}$ , was determined to be  $[\eta] = 8.1 \times 10^{-3} M_w^{0.704}$  with  $M_w$  in the units of g/mol and  $[\eta]$  in  $\text{cm}^3/\text{g}$ . However, it is not easy to determine the intrinsic viscosity of the Boger fluids via a Huggins extrapolation of directly measured shear viscosities because of the inherent imprecision of shear rheometry and the need to evaluate accurately the difference  $\Delta\eta/(\eta_s c) = (\eta_0 - \eta_s)/(\eta_s c)$  as  $c \rightarrow 0$ . Although styrene oligomer should act as an athermal solvent and result in near-theta conditions [Anna *et al.* (2001)], so far there have been no reliable reports of measured intrinsic viscosities for a pure polystyrene Boger fluid. Solomon and Muller (1996) report intrinsic viscosity measurements of polystyrene dissolved in a mixture of the theta solvent dioctylphthalate and styrene oligomer. They obtained an excluded volume exponent  $\nu$  of slightly less than the value of 0.5 expected for a theta solvent. The poorer solvent quality may be explained by a preferential attraction of the better of the two solvents in the solvent mixture towards the high polymer, and the contraction of the coil to reduce its expansion into the poorer-quality solvent [Larson (2005)]. In the following we use a Mark–Houwink–Sakurada relation with the excluded volume exponent of  $\nu = 0.52$  from [Anna *et al.* 2001] (corresponding to near theta conditions for our Boger fluids) and  $K_{[\eta]} = 0.02$  in order to determine intrinsic viscosities from the molar mass for our calculations of the critical concentration from Eq. (1). However, the solvent quality of Boger fluids is still not fully understood, and it should be borne in mind that the calculated Zimm times in the following are imprecise due to this uncertainty in the intrinsic viscosities.

To circumvent this difficulty in the definition of the critical concentration, in addition to Eq. (1) we have also included in Fig. 3 a purely geometrical calculation for the coil overlap conditions in Boger fluids, derived from the mean square size of a polymer coil in its random walk configuration [Graessley (1980); Kulicke and Clasen (2004)]:

**TABLE III.** Critical concentrations for the polystyrene/styrene oligomer solutions (Boger fluids) determined from the intrinsic viscosity [Eq. (1)], the radius of gyration [Eq. (27)] and from Eq. (41).

$M_w/(g/mol)$	$c^*/(g/cm^3)$	$c_{R_G}^*/(g/cm^3)$	$c_{min}/(g/cm^3)$
$8.27 \times 10^6$	$5.1 \times 10^{-3}$	$7.0 \times 10^{-3}$	$1.0 \times 10^{-6}$
$6.00 \times 10^6$	$6.2 \times 10^{-3}$	$8.2 \times 10^{-3}$	$1.7 \times 10^{-6}$
$5.67 \times 10^6$	$6.4 \times 10^{-3}$	$8.4 \times 10^{-3}$	$1.9 \times 10^{-6}$
$2.84 \times 10^6$	$7.0 \times 10^{-3}$	$1.2 \times 10^{-2}$	$3.5 \times 10^{-6}$
$1.80 \times 10^6$	$1.2 \times 10^{-2}$	$1.5 \times 10^{-2}$	$1.0 \times 10^{-5}$

$$c_{R_G}^* = \frac{M_w}{\frac{4}{3}\pi(R_G^2)^{3/2}N_A}. \quad (27)$$

The radius of gyration  $R_G$ , assuming near-theta conditions for the Boger fluids, can be calculated from molecular parameters including the C–C bond length  $b$ , the monomer molar mass  $M_u$ , and the characteristic ratio  $C_\infty$  for a given polymer [Kulicke and Clasen (2004)],

$$R_G = \sqrt{\frac{b^2 C_\infty M_w}{3M_u}}. \quad (28)$$

For polystyrene  $b=0.154$  nm,  $C_\infty=9.6$ , and  $M_u=104$  g/mol. The critical overlap concentrations  $c^*$  and  $c_{R_G}^*$  for the solutions of polystyrene/styrene oligomer and  $c^*$  for the solutions polystyrene (PS)/DEP studied in the present work are listed in Tables III and IV.

The measured relaxation times for the PS/DEP solutions in Fig. 3 span the range from close-to, or above, the critical concentration into the semidilute regime, whereas the measured relaxation times of the Boger fluids lie in a regime below even the most conservative definition of  $c^*$ . In these dilute solutions the relaxation times of isolated coils should be *independent* of the concentration according to Eq. (26). In contrast to this expectation, the experimental relaxation times show a strong and monotonic decrease as the concentration is reduced to well below the critical overlap concentration. Similar observations of concentration dependent relaxation times in capillary thinning experiments below  $c^*$  have recently been reported by Bazilevskii *et al.* (2001) and Stelter *et al.* (2002) for polyacrylamide in water/glycerol mixtures and by Tirtaatmadja *et al.* (2006) for polyethylene oxide in water/glycerol mixtures.

**TABLE IV.** Critical concentrations for the polystyrene/DEP solutions, determined from the intrinsic viscosity [Eq. (1)] and from Eq. (41).

$M_w/(g/mol)$	$c^*/(g/cm^3)$	$c_{min}/(g/cm^3)$
$8.27 \times 10^6$	$1.6 \times 10^{-3}$	$8.4 \times 10^{-7}$
$5.67 \times 10^6$	$2.1 \times 10^{-3}$	$1.5 \times 10^{-6}$
$2.84 \times 10^6$	$3.5 \times 10^{-3}$	$4.5 \times 10^{-6}$



## B. Small amplitude oscillatory shear

Capillary thinning experiments yield the characteristic relaxation-controlled unraveling time associated with strong flows and large molecular deformations. These values may also be compared to the relaxation times measured for each fluid in weak flows and small deformation conditions. Lindner *et al.* (2003) calculated relaxation times for dilute aqueous solutions as low as 250 ppm from normal stress data fitted to an appropriate constitutive equation, and found good agreement with the expected Zimm relaxation times. However, for the Boger fluids investigated in this report the elastic response can be directly observed to even lower concentrations using small amplitude oscillatory shear (SAOS) flow [Anna *et al.* (2001)]. The Zimm relaxation times for the polystyrene Boger fluids have been obtained from regressing the expressions for the linear viscoelastic moduli  $G'$  and  $G''$  [Eqs. (2) and (3)] to the measured experimental data. A representative example of the resulting fits to the oscillatory shear data is presented in Fig. 4(a). At low frequencies the elastic modulus is dominated by the Zimm spectrum of the high molar mass polystyrene solute, allowing for unambiguous determination of the longest relaxation time  $\tau_0$ , while at high frequencies the response is dominated by the weak elasticity of the oligomeric solvent.

However, with progressively decreasing concentration, the elastic modulus  $G = cRT/M_w$  of the solute decreases and the contribution of the high molar mass polystyrene to the measured elastic moduli is increasingly obscured by the oligomer. This can be seen in the data presented in Fig. 4(b) for a dilution series of a single molar mass of polystyrene. Consequently, accurate fitting of the Zimm spectrum is hindered at low concentrations and the extraction of an accurate longest relaxation time  $\tau_0$  becomes less robust.

For low frequencies,  $\tau_s\omega \ll 1$ , the first term in Eq. (2) can be neglected and the expression reduces to the pure Zimm spectrum. The longest relaxation times obtained from the fits for each fluid can then be used to verify the expected scaling of the reduced storage modulus  $G'M_w/cRT$  with the reduced frequency  $\tau_0\omega$ :

$$\frac{G'M_w}{cRT} \sim \sum_{i=1}^{N_{\text{modes}}} \left[ \frac{(\tau_0\omega)^2}{i^{4+2\tilde{\sigma}} + (\tau_0\omega)^2} \right]. \quad (29)$$

Figure 4(c) shows the reduced moduli for the fluids used in the present study that exhibited sufficient elastic response from the polystyrene solute to perform satisfactory fits to Eq. (2). The underlying Zimm spectrum can clearly be observed in Fig. 4(c) from the common mastercurve at low reduced frequencies ( $\tau_0\omega \ll 1$ ).

The longest relaxation times obtained from this analysis are represented in Fig. 5 as dimensionless values  $\tau_0/\tau_z$  plotted as a function of  $c/c^*$  [with  $c^*$  being the critical concentration from Eq. (1)]. To obtain the Zimm relaxation time  $\tau_z$  (assuming a Zimm spectrum for the isolated polymer coil in a solvent), the universal ratio in Eq. (26) can easily be calculated from Eq. (4) to give

$$U_{\eta r} = \frac{\sum_i \tau_i}{\tau_0} \cong \sum_i \frac{1}{i^{2+\tilde{\sigma}}}, \quad (30)$$

where  $\tilde{\sigma}$  is given by the Thurston relation, Eq. (5), giving a Zimm relaxation time  $\tau_z$  of

$$\tau_z = \frac{1}{\sum_i \frac{1}{i^{2+\tilde{\sigma}}}} \frac{[\eta] \eta_s M_w}{RT}. \quad (31)$$

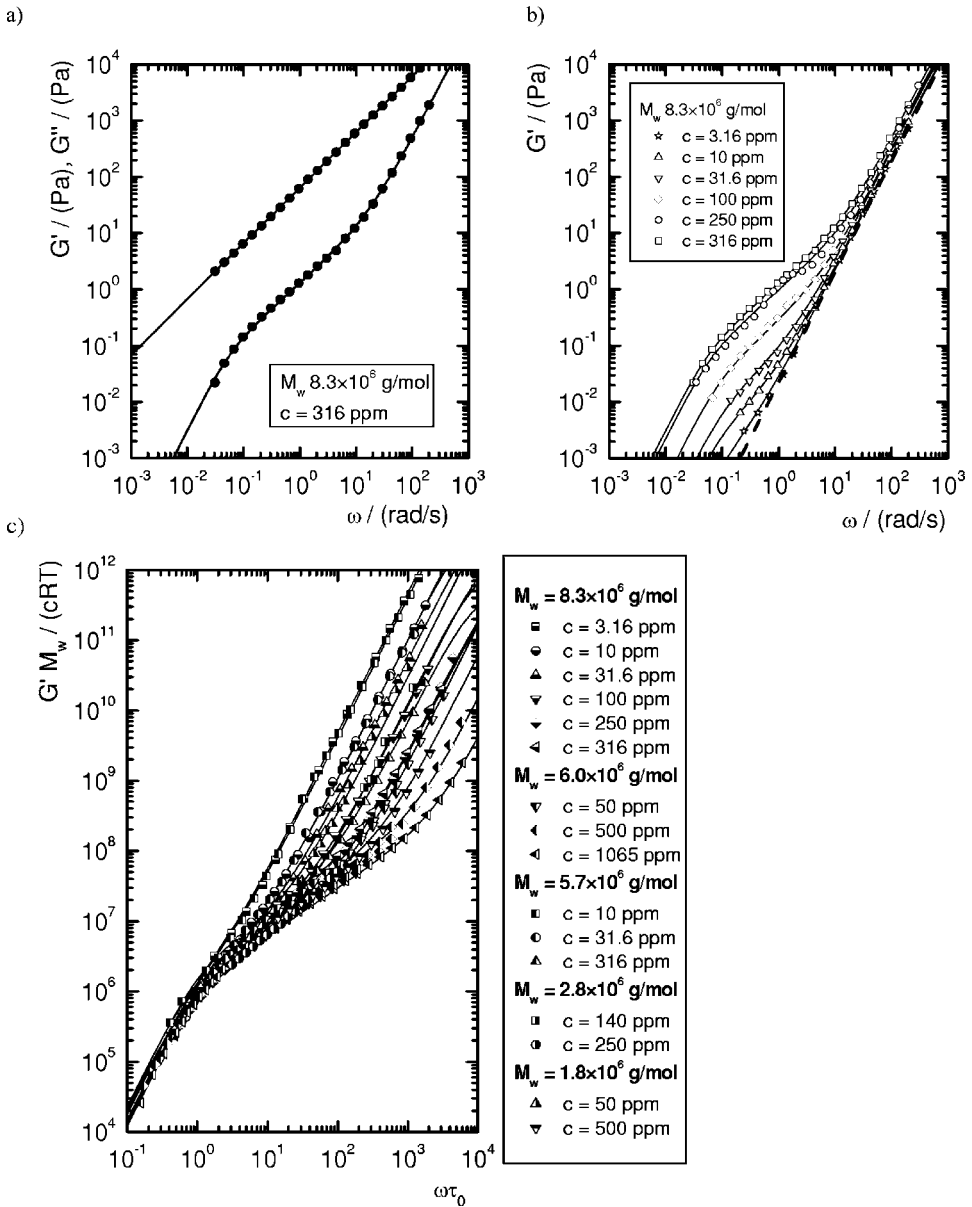


**FIG. 4.** (a) Experimentally observed loss modulus  $G''$  (upper curve) and storage modulus  $G'$  (lower curve) as a function of the angular frequency  $\omega$  for a polystyrene dissolved in styrene oligomer (symbols) as well as the fits of Eqs. (2) and (3) to the experimental data (lines). (b) Storage moduli  $G'$  as a function of the angular frequency  $\omega$  for different concentrations of polystyrene dissolved in styrene oligomer. In addition the fits of Eq. (2) to the experimental data are shown (lines). The lowest (dashed) line depicts the response of the pure oligomeric solvent which is weakly elastic with  $\tau_s \approx 6.5 \times 10^{-4}$  s. (c) Reduced storage moduli  $G'M_w/(cRT)$  as a function of the reduced frequency  $\omega\tau_0$  for polystyrenes of different molar masses and concentrations. The longest relaxation times  $\tau_0$  were determined from fits of Eqs. (2) and (3) to the experimental data as shown in Fig. 4(a).

The resulting values of  $\tau_Z$  for each fluid are given in Tables I and II. It is clear from Fig. 5 that at low concentrations the Zimm relaxation time is recovered accurately from SAOS experiments. Approaching the critical concentration, the relaxation time slowly

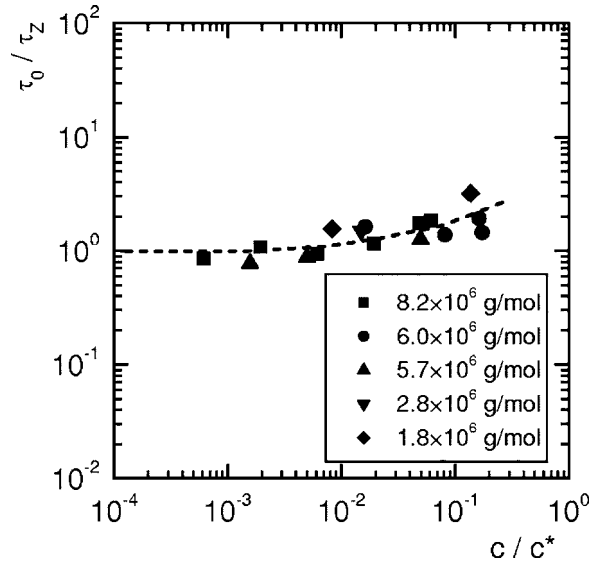


**FIG. 5.** Reduced relaxation time  $\tau_0/\tau_z$  as a function of the reduced concentration  $c/c^*$ , determined from SAOS experiments and fits of the moduli to Eqs. (2) and (3) for polystyrene of different molar masses dissolved in styrene oligomer.

increases due to the growing importance of intermolecular interactions with increasing concentration. The form of the mastercurve in Fig. 5 can be rationalized by noting that the polymeric contribution to the viscosity  $\eta_p$  in Eq. (26) can be expanded in the concentration as for example by the Martin equation [Kulicke and Clasen (2004)]:

$$\eta_p = \eta_s c [\eta] e^{K_M c [\eta]}, \tag{32}$$

where  $K_M$  is the Martin coefficient. In combination with Eqs. (1), (12), (26), (30), and (31) this gives a dependence of the longest relaxation with the reduced concentration  $c/c^*$  of the form

$$\tau_0 = \frac{1}{U_{\eta\tau}} \frac{[\eta] \eta_s M_w}{RT} \exp\left(K_M 0.77 \frac{c}{c^*}\right) = \tau_z \exp\left(K_M 0.77 \frac{c}{c^*}\right). \tag{33}$$

Using this approach, one can also plot the longest relaxation times obtained from the capillary thinning experiments in their reduced form  $\tau_0/\tau_z$  as a function of  $c/c^*$  as shown in Fig. 6. The superposition of data for different molar masses shows the expected scaling of the longest relaxation time  $\tau_0 \sim M_w^{3\nu}$  obtained from the definition of the Zimm relaxation time in Eq. (31) with molar mass and solvent quality.

However, comparing this mastercurve to the relaxation times determined from the SAOS experiments of Fig. 5 (depicted as a broken line in Fig. 6), two important distinctions are noted. First, the relaxation times in uniaxial extension deviate at much lower concentrations from the asymptotic value given by the Zimm theory in comparison to the small amplitude oscillatory shear experiments. In addition, the data in Fig. 5 indicates that at very low concentrations the relaxation time determined from capillary thinning appears to fall below the Zimm relaxation time. This puzzling observation is in agreement with observations made by Bazilevskii *et al.* (2001) for very dilute polyacrylamide/

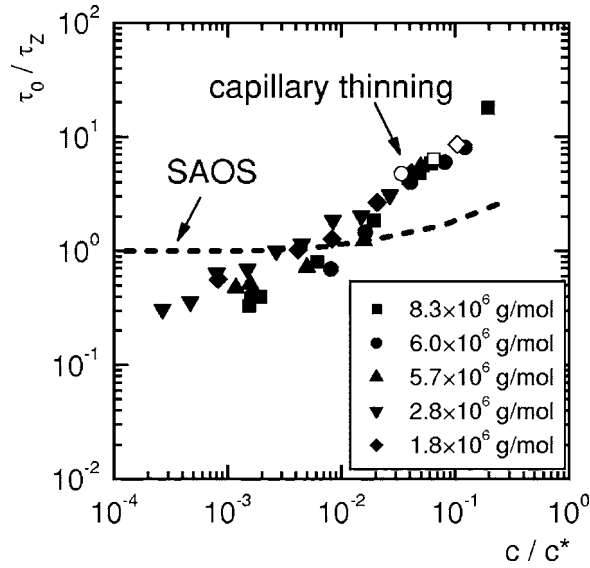


**FIG. 6.** Reduced relaxation time  $\tau_0/\tau_z$  as a function of the reduced concentration  $c/c^*$  for several dilution series of polystyrene Boger fluids determined from capillary break thinning experiments. In addition to the data obtained in this work, data points for the boger fluids SM1 ( $2 \times 10^6$  g/mol,  $\circ$ ), SM2 ( $6.5 \times 10^6$  g/mol,  $\square$ ), and SM3 ( $20 \times 10^6$  g/mol,  $\diamond$ ) are shown (taken from [7] and [20]). For comparison, also a mean square fit to the results from the SAOS experiments in Fig. 5 is shown.

water/glycerol solutions. For an explanation of this peculiar phenomenon, one needs to examine in greater detail the thinning dynamics at very low concentrations as we show later.

### C. Transient stress evolution

In general, lowering the concentration of a polymer in solution so that the relaxation time approaches its limiting Zimm relaxation time leads to the question of whether the flow in the thinning filament is still dominated by the timescale of the polymer or by that of the viscopillary flow in the Newtonian solvent. A discussion of these time scales is given by [McKinley (2005)]. For viscous Newtonian fluids the relevant timescale is the viscous capillary breakup time  $t_{\text{visc}} = \eta_0 D_0 / (2\gamma)$ . The ratio of this time scale to the longest relaxation time  $\tau_0$  in the polymer defines the elastocapillary number

$$Ec = \frac{\tau_0}{t_{\text{visc}}} = \frac{2\tau_0\gamma}{\eta_0 D_0}. \quad (34)$$

For elastocapillary numbers below unity, the elastic stresses from the polymeric contribution to the observed flow are negligible compared to the viscous stresses and a capillary thinning experiment will not allow the extraction of a polymeric relaxation time. For dilute solutions, the polymeric contribution to the elastocapillary number is principally through the molar mass dependence of the relaxation time. We therefore expect a lower limit in the molar mass for a given experimental setup with specified values of the surface tension  $\gamma$ , solvent viscosity  $\eta_0$ , and initial radius.

However, even for  $Ec > 1$ , observation of a filament thinning process dominated by the elasticity [as indicated by a corresponding exponential decrease of the filament diameter according to Eq. (22)] may not be possible if the concentration is not high enough. The

transition from the initial balance of capillary and viscous stresses to the balance of capillary and elastic forces is progressively shifted to later times, as the polymer concentration  $c$  and the elastic modulus  $G$  are progressively reduced [see Eqs. (12) and (20)]. Physically, it is clear that if the polymer concentration is too small the elastic stress term on the right hand side of Eq. (20) cannot balance the squeezing action arising from capillary pressure. Instead viscous stresses from the oligomeric solvent provide the dominant resistance to thinning. Because the elastic stresses evolve nonlinearly (exponentially) with time, it is not straightforward to determine the crossover conditions from a simple order of magnitude scaling estimate and instead we turn to numerical calculations.

In the left hand column of Figs. 7(a)–7(c) we show the temporal variation in the different contributions to the overall stress, obtained from the numerical integration of Eqs. (17)–(20), for three different concentrations of the same polymer. The capillary pressure, which drives the flow, increases monotonically in time and ultimately diverges at a critical timescale interpreted as the breakup time,  $t_{br}$ . The dashed and dotted lines show the relative contributions of the viscous and elastic stresses, respectively. As the concentration is lowered, the transition from a solvent dominated to an elasticity dominated flow shifts to later times during the thinning process. While this shifts the elasto-capillary regime to smaller radii and therefore towards the lower resolution limit of the experimental setup, it also means a faster approach to the finite extensibility limit of the polymer.

In the right hand column of Figs. 7(a)–7(c) we show the individual modal contributions to the polymer stretch tensor  $\mathbf{A}$  as a function of time scaled by the longest relaxation time. For the bulk of the capillary thinning process, the majority of the stress is carried by the longest mode ( $i=1$ ). Exponential decay in the radius corresponds directly to exponential growth in the principal stretch difference  $A_{zz,1} - A_{rr,1}$  of the longest mode. As the deformation rate diverges close to the singular breakup event, the shorter modes begin to stretch rapidly and ultimately all modes approach their relevant finite extensibility limit. Once the higher modes of the configuration  $\mathbf{A}$  reach their finite extensibility limit, the flow pattern again crosses over to a Newtonian-like flow behavior. Extraction of a relaxation time by a simple exponential fit to Eq. (22) is therefore not possible once finite extensibility effects start to dominate the flow. At low concentrations, the combined effects of finite extensibility and a low initial concentration or modulus eliminate the possibility of a clear elastocapillary balance at the microscale or a macroscopic detection of an exponential decay regime in this rheometric device, even though there is a well-defined underlying microscopic relaxation time for the fluid itself. This is also demonstrated in Fig. 8 by a series of numerical calculations for a progressively diluted polystyrene Boger fluid. The longest relaxation time  $\tau_0$  for these calculations is chosen to be constant for all dilutions and the value is assumed to agree with the Zimm time  $\tau_z$ . As one can see, the breakup times progressively decrease with decreasing concentration. At a concentration of  $c=100$  ppm ( $c/c^*=0.012$ ) there is a clear region of elastocapillary decay and a filament decay rate that would agree with the expected rate  $1/(3\tau_0)$ . However, the slopes of the curves in the intermediate thinning regime appear to become steeper in the semilog plot of Fig. 8 and this suggests apparent relaxation times that are *below* the Zimm time used for these calculations. This effect is further amplified by a gradual “smearing out” of the transition from the initial Newtonian thinning to the elastocapillary regime.

#### D. The critical concentration $c_{min}$

It is clear from the above model calculations that capillary thinning instruments have a minimum detectable elasticity limit, in much the same way that conventional torsional

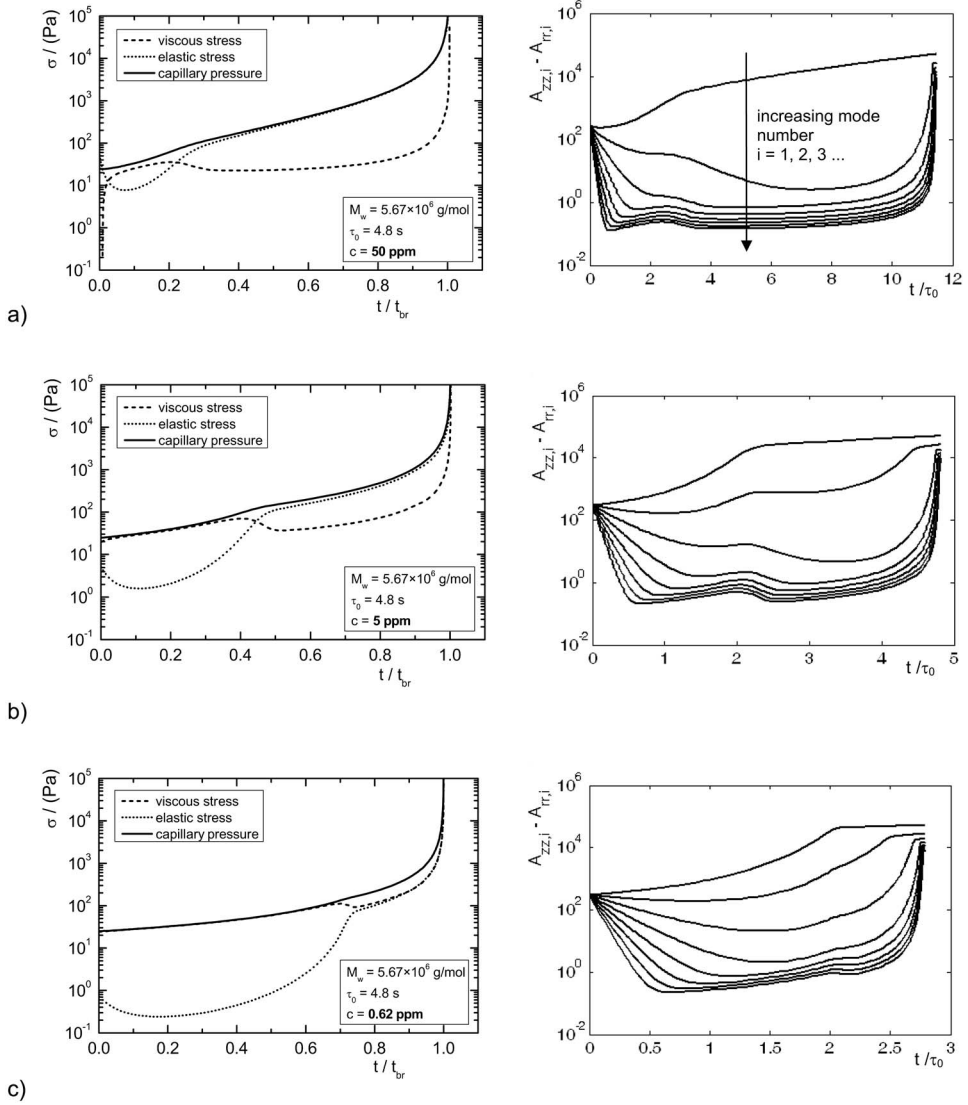


**FIG. 7.** Stress distribution in capillary breakup experiments. Shown are the driving capillary pressure and the stress distribution between the solvent and the polymer. Results were obtained from numerical calculations for three different concentrations  $c$  of polystyrene in styrene oligomer for a constant Zimm relaxation time. The initial diameter of the filament was assumed as  $D_0=2.39$  mm in accordance with experimental observations. The filament breakup times were (a)  $t_{br}=11.41 \cdot \tau_0$ , (b)  $t_{br}=4.81 \cdot \tau_0$ , and (c)  $t_{br}=2.82 \cdot \tau_0$ . The right hand side shows the respective evolution of the chosen 8 modes of the configuration  $(A_{zz,i}-A_{rr,i})$ , with an increasing mode number  $i$  from top to bottom.

reometers used in SAOS tests have a minimum value of elastic modulus that can be reliably detected. The ultimate limit of the capillary thinning experiment for the observation of the polymeric contribution can be seen in Fig. 7(c). Even though all modes of the polymer stretch have reached their finite extensibility limit at late times, the contribution of the viscous stresses from the solvent still dominates the flow behavior. The

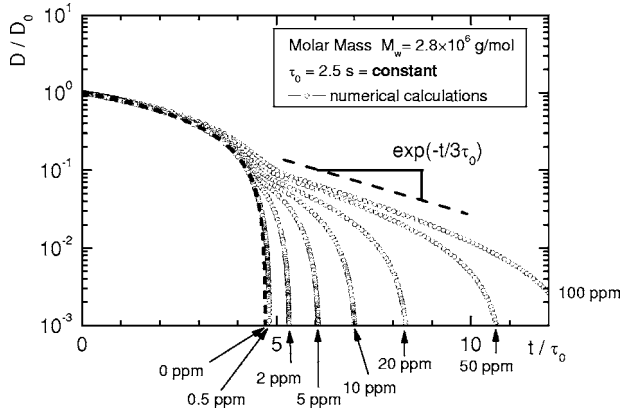


**FIG. 8.** Numerical calculations of the diameter  $D/D_0$  as a function of the reduced time  $t/\tau_0$  for a dilution series of polystyrene in styrene oligomer. Even though the longest relaxation time  $\tau_0$  is held *constant* for all calculations, only the calculations for the highest concentrations show a profile in accordance with the indicated slope of  $\exp(-t/3\tau_0)$  of Eq. (22).

minimum concentration at which the total elastic stress of the fully expanded coils just balances the viscous stresses of the solvent can be estimated from the force balance in Eq. (9).

Following Entov and Hinch (1997), close to the finite extensibility limit we expect  $A_{zz} \gg A_{rr}$  and a negligible temporal change of the polymer stretch  $A_{zz}$ , the relevant evolution equation [Eq. (17)] then reduces to

$$2\dot{\epsilon}_{zz,i} = \frac{1}{\tau_i} f_i A_{zz,i}. \quad (35)$$

This gives for the finite extensibility factor  $f_i$ :

$$f_i = 2\dot{\epsilon} \tau_i \quad (36)$$

and with  $\text{tr}\mathbf{A} \approx A_{zz}$  a solution for  $A_{zz}$  at the finite extensibility limit

$$A_{zz,i} = L_i^2 \left( 1 - \frac{1}{2\dot{\epsilon} \tau_i} \right). \quad (37)$$

Substituting Eqs. (36) and (37) into the equation for the polymeric contribution to the stress  $\Delta\sigma_p$  [Eq. (10)] with  $A_{zz} \gg A_{rr}$  we obtain for the finite extensibility limit

$$\Delta\sigma_p = \sum_i^{N_m} 2G\dot{\epsilon} \tau_i L_i^2 \left( 1 - \frac{1}{2\dot{\epsilon} \tau_i} \right). \quad (38)$$

As the filament radius approaches zero, the stretch rate diverges and the final term becomes negligible. Also neglecting the marginal contribution of the higher modes of the spectra for relaxation time  $\tau_i$  [Eq. (4)] and finite extensibility  $L_i^2$  [Eq. (15)] we finally obtain the following expression for the polymer stress once the longest mode has reached its finite extensibility limit:

$$\Delta\sigma_p \approx 2G\dot{\epsilon} \tau_z L^2. \quad (39)$$

From this we obtain a constant polymer extensional viscosity  $\eta_E \approx 2G\tau_z L^2$  for the finite extension limit. The viscous stress carried by the solvent will dominate at late times



if the term  $3\eta_s\dot{\epsilon}$  in Eq. (9) becomes larger than the polymer stress  $\Delta\sigma_p$  given by Eq. (39). The polymer contribution to the total stress is thus only observable in capillary thinning experiments if

$$\frac{2G\tau_z L^2}{3\eta_s} > 1. \quad (40)$$

Substituting the modulus from Eq. (12), we derive an expression for the lowest possible polymer concentration for an observable elastic contribution to a capillary breakup experiment. We denote this concentration  $c_{\min}$  and require

$$c > c_{\min} = \frac{3}{2} \frac{M_w \eta_s}{RT\tau_z L^2} \quad (41)$$

or by combining this expression with the Zimm relaxation time given by Eq. (31):

$$c > c_{\min} = \frac{3}{2} \frac{U_{\eta\tau}}{[\eta]L^2}. \quad (42)$$

At this critical concentration  $c_{\min}$  the extended polymer is still contributing partially to the overall stress at late times, however, this concentration marks the point below which the polymer will carry less stress than the solvent even if it is fully extended. It should be noted that  $c_{\min}$  differs from the critical overlap concentration  $c^*$  for the equilibrium configuration principally by the factor  $1/L^2$  since Eq. (42) reduces with Eq. (1) to  $c_{\min} = 1.94U_{\eta\tau}c^*/L^2$  and  $c_{\min}$  is therefore orders of magnitude smaller than  $c^*$ .

The critical concentrations  $c_{\min}$  for the polystyrene solutions can easily be calculated from molecular parameters and are shown in Table III. The value of  $c_{\min}$  was also chosen for the numerical calculation in Fig. 7(c) and it can clearly be seen that at  $c=c_{\min}$  the viscous and polymeric stresses provide the same contribution to the overall stress balance at late times. The critical concentration  $c_{\min}$  is also indicated in Figs. 2(b) and 14(b) in addition to the experimental thinning data. This theoretical estimate for the critical concentration describes quite well the borderline between purely viscous thinning behaviour and the onset of significant elastocapillary effects for all three molar masses.

## E. Relaxation times from numerical calculations

Given these limitations to directly extracting the relaxation time from elastocapillary thinning, we have also used a different approach to obtain good estimates of the relaxation times close to the critical concentration limit  $c_{\min}$  given by Eq. (41). Numerical integrations of Eqs. (17)–(20) for the filament thinning process with the longest relaxation time  $\tau_0$  as the only adjustable parameter are used to obtain the best agreement with the experimentally measured filament thinning profiles first presented in Fig. 2. Samples of the resulting best fits to the experimental data are shown for several decades of concentration and two different molar masses in Figs. 9 and 10. It is clear that excellent agreement with the measured diameter data can be achieved by adjusting the value of  $\tau_0(c)$ , even though the profiles of the stress evolution are not elastically dominated at low concentrations.

The relaxation times derived from these numerical calculations in Figs. 9 and 10 can also be used to regenerate the reduced data or master curve originally presented in Fig. 6. These new results are presented in Fig. 11 and it is clear that the true relaxation time in uniaxial extension asymptotically approaches a constant value at low concentrations in accordance with the concentration-independent relaxation times directly measured with the SAOS experiments at low concentrations. However, one must note that the constant

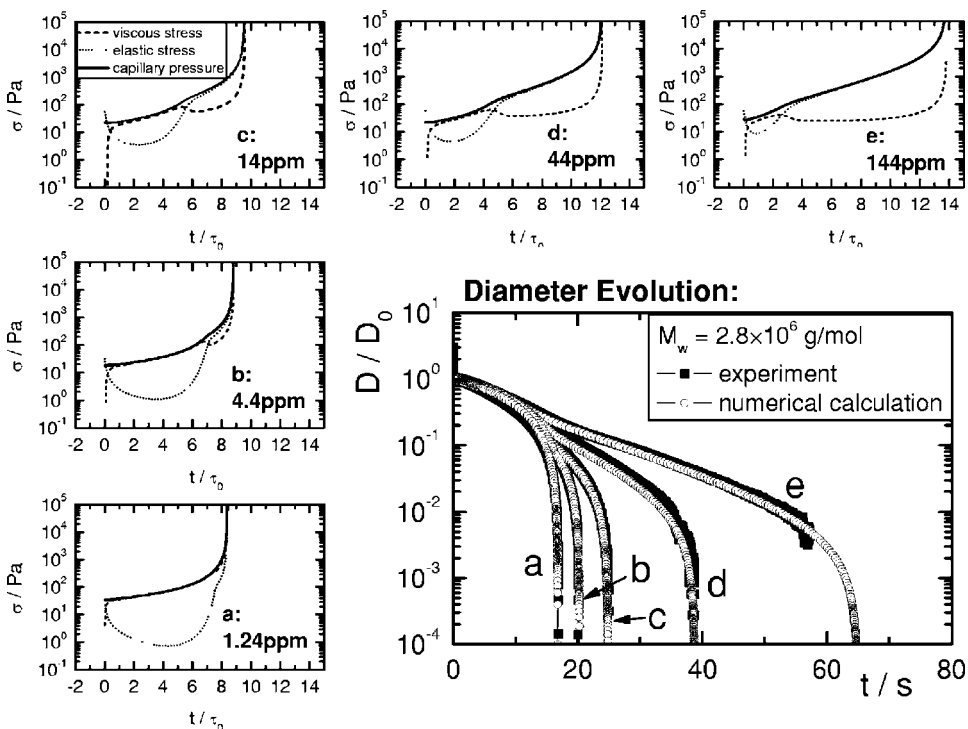


**FIG. 9.** Comparison of the numerically calculated diameter evolution with experimental observations for a dilution series of a polystyrene Boger fluid with a molar mass  $M_w = 2.8 \times 10^6$  g/mol. The initial diameters for the numerical calculations were taken from the experimental observations. In addition, the calculated evolution in stress distribution is given for each concentration. The critical concentration from Eq. (41) is  $c_{\min} = 1.7$  ppm.

value of the reduced relaxation times obtained from our numerical calculations for molecular unraveling in uniaxial extension is slightly lower than unity: the average molecular relaxation-controlled unraveling time from Fig. 11 at low concentrations is a factor of  $\sim 1.3$  lower than the corresponding Zimm relaxation times. This differential is probably a consequence of describing the unraveling chain as a suspension of uncoupled dumbbells. We do this for computational simplicity only; a more realistic description would treat the chain as a fully coupled set of discrete relaxation modes or through Brownian dynamics simulations [Doyle *et al.* (1997); Ghosh *et al.* (2001)].

## F. Enhanced relaxation times in extensional flow

The relaxation times obtained from the numerical calculations of transient uniaxial flow at higher concentrations are, as expected, in very good agreement with the relaxation times directly extracted from the fit of Eq. (22) to the experimental data. Still, these values are substantially higher than the relaxation times obtained from the oscillatory shear flow experiments.

This can also be observed in the data presented in Fig. 12 for solutions of polystyrene in the good solvent diethylphthalate. Since the DEP solutions have a much smaller viscosity than the Boger fluids, the observable range of relaxation times is shifted to higher concentrations, as determined by the low viscosity limit of the elastocapillary number in Eq. (34). For these solutions it is not possible to obtain relaxation times close to the

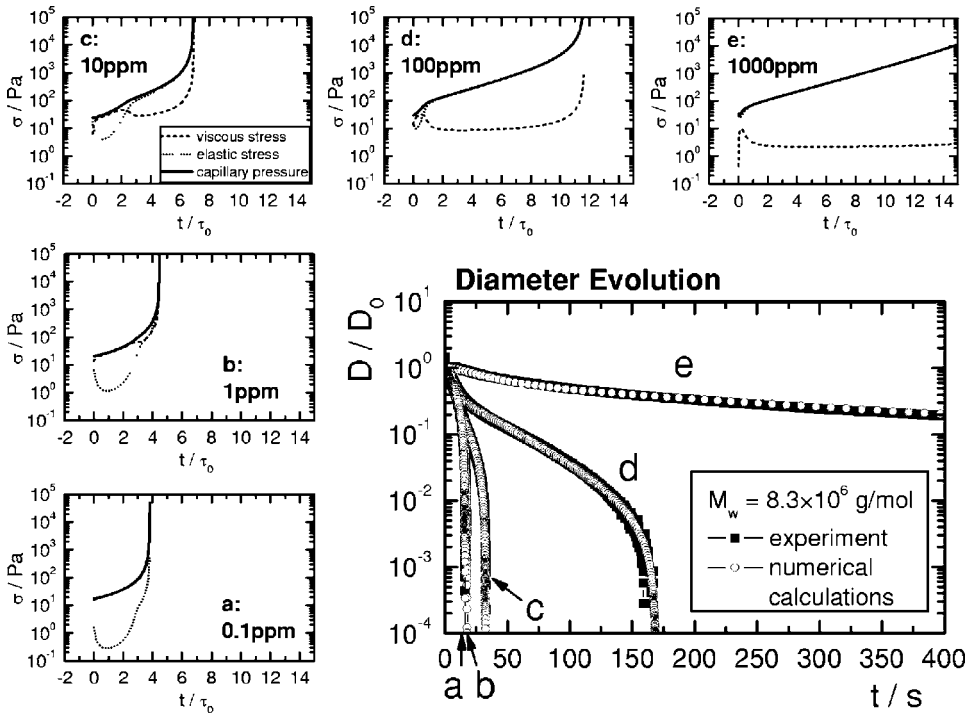


**FIG. 10.** Comparison of the numerically calculated diameter evolution with experimental observations for a dilution series of a Boger fluid with a molar mass  $M_w = 8.3 \times 10^6$  g/mol. The initial diameters for the numerical calculations were taken from the experimental observations. In addition, the calculated stress distribution is given for each concentration. The critical concentration from Eq. (41) is  $c_{\min} = 0.36$  ppm.

Zimm limit by capillary thinning or via SAOS experiments. However, we are able to determine the numerical value of the constant in the structure-property relationship of Eq. (32) to be  $K_M = 0.35$  by regression to the experimental viscometric data as shown in Fig. 13. For these DEP solutions, the intrinsic viscosities can be directly determined and used in the subsequent calculation of  $c^*$ . The corresponding prediction for the concentration dependence of the longest relaxation time [as given by Eq. (33)] is also shown in Fig. 12 by the solid line. Again, it can be seen that the relaxation times determined from capillary thinning start to rise above the dilute limit at much smaller concentrations than theoretically expected from Eq. (33).

The onset point for the increase in the characteristic relaxation times for elongational flow gives a rough estimate of a critical concentration for ultradilution  $c^\infty$ . Below this concentration (but still above the experimental sensitivity limit  $c_{\min}$ ) we are able to observe the presence of the polymer in terms of a delayed breakup time and a deviation from the thinning behavior of the viscous Newtonian solvent. The relaxation time or, more descriptively, the molecular relaxation-controlled unraveling time is, in this case, constant and corresponds to that of the single polymer coil. With further decreases in the solute concentration the transition to an elastocapillary balance shifts to progressively later times and smaller filament diameters. It thus becomes increasingly hard to resolve, given the optical constraints of the experimental instrumentation.

Above the ultradilution point  $c^\infty$  the concentration of the polymer coils is high enough that the long-range interactions between unraveling polymer coils leads to an increase in

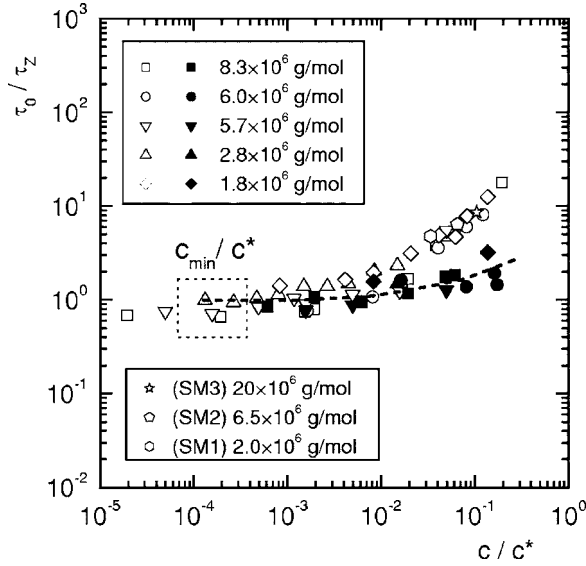


**FIG. 11.** Reduced relaxation times  $\tau_0/\tau_z$  as a function of the reduced concentration  $c/c^*$ , obtained from best fits of the numerically calculated diameter evolution to the experiments presented in Fig. 2 with  $\tau_0$  as an adjustable parameter (hollow symbols). For comparison, also the results from the SAOS experiments in Fig. 7 are given (filled symbols). Also the range of critical concentrations  $c_{min}/c^*$  for the different molar masses is indicated by the rectangle.

the effective relaxation time of the solution. The scaling of the relaxation time with the reduced concentration in this regime appears to obey the following relation proposed by Tirtaatmadja *et al.* (2006):

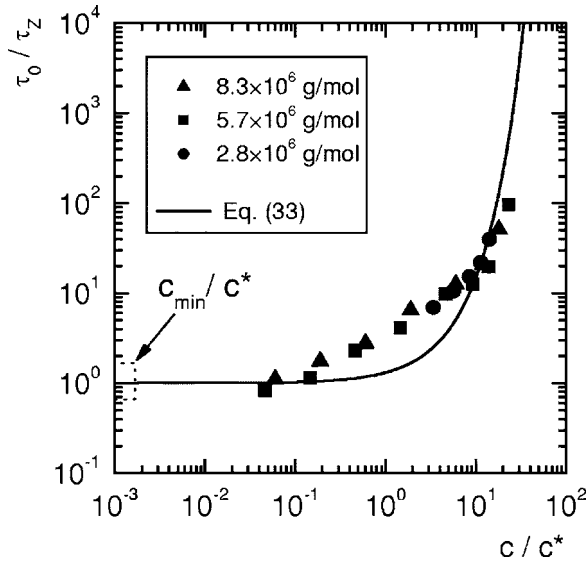


**FIG. 12.** Reduced relaxation times  $\tau_0/\tau_z$  as a function of the reduced concentration  $c/c^*$  for dilution series of polystyrene in DEP. In addition, the theoretical concentration dependence of the relaxation time according to Eq. (33) is shown. Also the range of critical concentrations  $c_{min}/c^*$  for the different molar masses is indicated by the rectangle.

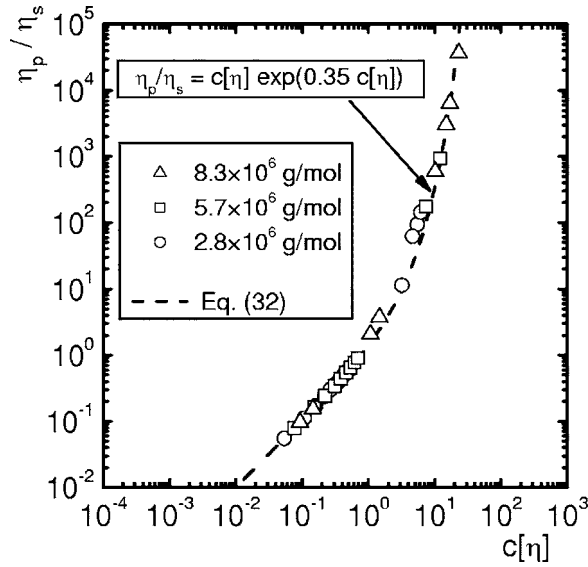


**FIG. 13.** Specific viscosity  $\eta_p/\eta_s$  as a function of the reduced concentration  $c[\eta]$  for solutions of polystyrene in DEP, determined with capillary viscometric measurements at lower concentrations, and cone-and-plate shear rheometry at higher concentrations. The continuous line gives the best fit to the structure-property relationship of Eq. (32).

$$\frac{\tau_0}{\tau_Z} \sim \left( \frac{c}{c^*} \right)^m \tag{43}$$

We determined an exponent of  $m=0.58$  in Fig. 12 for polystyrene in the relatively good solvent DEP in comparison to  $m=0.65$  observed by Tirtaatmadja *et al.* (2006) for PEO in glycerol/water mixtures. In contrast to this, for the polystyrene dissolved in the near theta solvent of styrene oligomer we obtain an exponent  $m=0.89$  from Fig. 11.

One possible explanation for the dependence of the power-law exponent  $m$  on the solvent quality can be obtained from scaling theory for unentangled semidilute solutions. In weak flows and for small molecular deformations close to equilibrium, such scaling theories are expected to hold only for concentrations above the overlap concentration  $c^*$ . However, for strong flows, such as those encountered in the present case of capillary thinning, the pervaded volume occupied by each expanding polymer coil increases rapidly due to unraveling. It is thus perhaps reasonable to imagine that we approach a semidilute state of polymer interaction in which neighboring chains overlap and interact. In such a regime, the scaling assumptions appropriate for semidilute “blob” theories should hold [Rubinstein and Colby (2003)]. This gives rise to a correlation length  $\xi \approx bg^{\nu}$ , where  $b$  is the monomer length and  $g$  is the number of monomers within the blob. On length scales shorter than the correlation length intrachain hydrodynamic interactions dominate; however, they are screened out on larger scales. Once the elongating polymer chains have expanded to become space filling, the concentration in an individual correlation blob should be equal to the overall solution concentration  $c \sim gb^3/\xi^3$  and the correlation length is thus

$$\xi \sim bc^{\frac{-\nu}{3\nu-1}} \tag{44}$$

The correlation length thus decreases with increasing concentration. Inside a correlation blob, single chain hydrodynamics dominate and therefore a Zimm relaxation time of the

**TABLE V.** Experimental and theoretical exponents  $m$  [Eq. (43)] and  $m_{\text{theory}}$  [Eq. (47)] for different solvent qualities.

	$\nu$	$m_{\text{theory}}$	$m$
PS Boger fluid	0.52	0.80	0.89
PEO in glycerol/water	0.55	0.54	0.65
PS in DEP	0.57	0.45	0.53

form given in Eq. (26) applies. The longest relaxation time  $\tau_\xi$  of a blob is proportional to the correlation volume  $\xi^3$  [Rubinstein and Colby (2003)] and therefore:

$$\tau_\xi \approx \frac{\eta_s}{k_B T} \xi^3 \sim \frac{\eta_s b^3}{k_B T} c^{\frac{-3\nu}{3\nu-1}}. \quad (45)$$

On length scales larger than  $\xi$ , the internal hydrodynamic interactions are screened out. We thus expect Rouse dynamics to dominate the chain-chain interactions of the expanded and overlapping coils. The relaxation time of the whole chain, consisting of  $M_w/(M_u g)$  blobs, each with a relaxation time  $\tau_\xi$ , thus has the following concentration dependence:

$$\tau_0 \approx \tau_\xi \left( \frac{M_w}{g M_u} \right)^2 \sim \frac{\eta_s b^3}{k_B T} \left( \frac{M_w}{M_u} \right)^2 c^{\frac{2-3\nu}{3\nu-1}}. \quad (46)$$

Finally, the coil overlap concentration can be substituted into Eq. (46) by noting that  $c^* \sim M_w^{1-3\nu}$  to obtain

$$\frac{\tau_0}{\tau_z} \sim \left( \frac{c}{c^*} \right)^{\frac{2-3\nu}{3\nu-1}}. \quad (47)$$

Comparing the exponent  $m$  from Eq. (43) with the exponent  $m_{\text{theory}} = (2-3\nu)/(3\nu-1)$  from Eq. (47) we are able to capture at least the general trend of observed slopes with the solvent quality as shown in Table V.

Stoltz *et al.* (2006) have recently investigated finite concentration effects in planar elongational flow using Brownian dynamics simulations. They also find that hydrodynamic interactions and excluded volume effects lead to a marked concentration dependence of the extensional rheological properties of supposedly dilute polymer solutions at concentrations as low as  $0.1c^*$ . Our data shown in Figs. 11 and 12 appears to be in good agreement with such findings.

## IV. CONCLUSIONS

In the experiments and calculations reported here, the relaxation times of a series of model dilute and semidilute polystyrene solutions have been determined over a wide range of concentrations and molecular weights in both shear flow and uniaxial extensional flow.

It should be noted that the experiments with very dilute solutions presented in this paper have been performed principally using very viscous solvents. The lack of data for very dilute (and therefore low viscosity) solutions of PS in DEP is a consequence of the Ohnesorge number  $\text{Oh} = \eta_0 / \sqrt{\rho \gamma R_0}$  being much less than unity. It is thus a balance of *inertia* and elasticity that controls the filament thinning-process in such solutions [McKinley (2005)], resulting in rapid rupture during the stretching phase or the formation of bead-on-string structures in capillary thinning experiments. These experimental difficul-

ties associated with low viscosity fluids are discussed in more detail by Rodd *et al.* (2005).

The linear viscoelastic properties of the dilute polystyrene solutions studied in this work are accurately described by the Zimm model, and the variation of the viscometric properties in the semidilute regime can be described by correlations such as the Martin equation. Capillary thinning measurements employing two different instruments show that in transient uniaxial extensional flow the effective relaxation time—or more accurately the molecular relaxation-controlled unraveling time—is a strong function of the polymer concentration, even at concentrations well below the conventional coil overlap concentration  $c^*$ . Interpretation of this finding must be approached with care because capillary thinning devices have a minimum sensitivity limit, just as any other rheometric device. A force balance shows that there is a critical concentration, denoted  $c_{\min}$ , below which polymeric stresses are insufficient to support the elastocapillary balance that is required for successful and unambiguous determination of the relaxation time.

Numerical calculations show that for concentrations close to  $c_{\min}$  the finite extensibility of the polymer chains and viscous stresses from the solvent lead to a systematic bias and underprediction of the true relaxation time of the polymer solution being tested. The widely used “elastocapillary balance”—which defines how the experimentally determined relaxation time of the solution is extracted—cannot be sustained below this critical concentration limit due to the magnitude of the underlying solvent stress and the finite extensibility of the chains. Consequently a spurious concentration dependence of the macroscopically measured relaxation time is obtained, even though the microscopic properties of the solution are unchanged.

Provided that the limit  $c < c_{\min}$  is avoided, capillary thinning measurements—in conjunction with numerical calculations—show that the fitted relaxation times are in good agreement with both the Zimm relaxation times determined from molecular theory and those obtained from small amplitude oscillatory shear measurements of the linear viscoelastic moduli. However, as the concentration is slowly increased over the range  $c_{\min} \leq c \leq c^*$ , the value of the molecular relaxation-controlled unraveling time characterizing transient elongation increases substantially above the relaxation time that is predicted theoretically or measured under near-equilibrium conditions, with the concentration of ultradilution  $c^\infty$  as the onset point of this substantial rise. Recent Brownian dynamics simulations incorporating excluded volume effects and interchain hydrodynamic interactions in planar elongational flows also show similar finite concentration effects for  $0.1c^* \leq c \leq c^*$  [Stoltz *et al.* (2006)].

In our analysis of the elastocapillary thinning process, we have relied on the multi-mode suspension of FENE-P dumbbells proposed by Entov and Hinch (1997). However, this relatively simple closed-form constitutive model does not incorporate the progressive changes in the hydrodynamic interaction (HI) between different segments of an elongating polymer chain. Neglecting such effects may be unwarranted in the present flow because we have demonstrated that polymer chains reach their full extension during the necking process, and the magnitude of the corresponding elastic stress determines the minimum concentration above which we can measure the extensional rheology of a dilute polymer solution. The role of conformation-dependent hydrodynamic interaction has been considered recently by Prabhakar *et al.* (2006) using a more complex set of finitely extensible bead-spring equation (the so called twofold normal approximation) in which the functional form of the evolution equations for the coupled FENE springs have been carefully verified using Brownian dynamics simulations that incorporate HI. This detailed study shows that the large changes in the molecular elongation of the chain can lead to conformational hysteresis; i.e., elongated polymer molecules remain extended even when



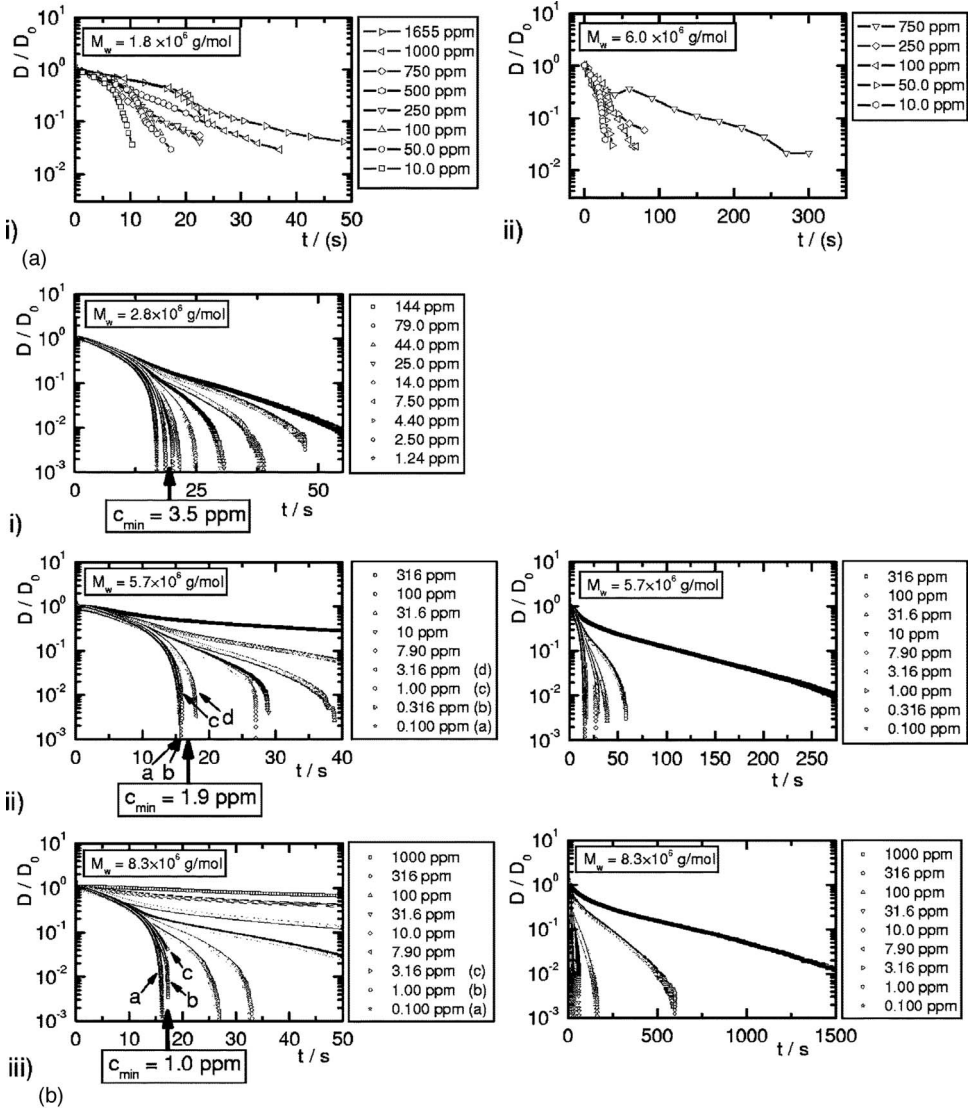


FIG. 14. Reduced diameter  $D/D_0$  as a function of time  $t$  in capillary thinning experiments for several dilution series of narrowly distributed polystyrene samples dissolved in: (a) styrene oligomer, determined from CCD camera video images; (b) styrene oligomer, determined with a laser micrometer. In addition to the experimental data, (b) also shows the theoretical critical concentrations  $c_{min}$  calculated from Eq. (41) that depict the minimum concentration for an observable influence of polymer on the capillary thinning behavior; and (c) DEP, determined with a laser micrometer.

the local extension rate drops below the critical value required for the initial onset of chain stretching [Schroeder *et al.* (2003)]. This complex hysteretic effect in turn modifies the elastocapillary thinning process from the single exponential response of Eq. (22) which corresponds to  $\dot{\epsilon} = 2/(3\tau_0)$ . However, Prabhakar *et al.* also show that direct measurement of the rate of change in the mid-plane diameter  $D(t)$  can still be used to directly probe the elastic stress in the elongating fluid filament and thus to measure the transient elongational viscosity of a dilute polymer solution.

When the characteristic time constant determined experimentally for a wide range of

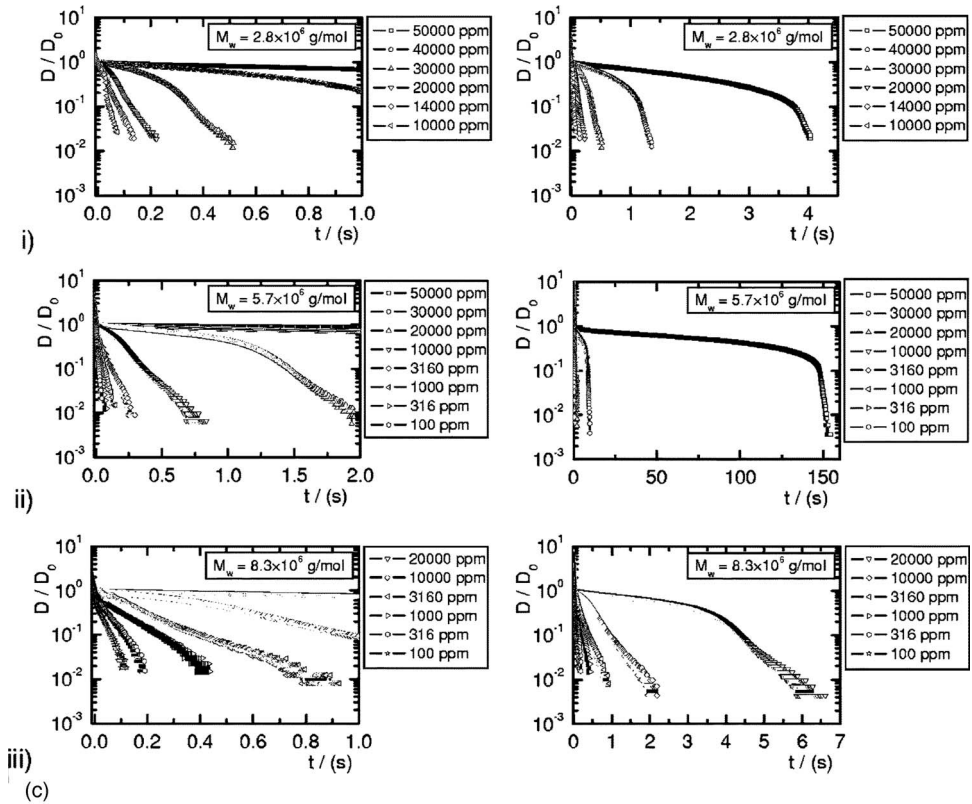


FIG. 14. (Continued).

molecular weights is normalized with the Zimm time constant, the result is found to increase according to a power law in the reduced concentration  $c/c^*$ , with an exponent that varies with the thermodynamic quality of the solvent. This power-law scaling with the reduced concentration appears to be approximately consistent with treating the dynamics of unraveling and overlapping polymer chains within the framework of blob scaling theories for semidilute solutions.

## ACKNOWLEDGMENTS

The portion of this research carried out at MIT was supported by the NASA Microgravity Fluid Dynamics program (Code UG) under Grant No. NCC3-610. M.O. acknowledges financial support from the Industrial Partnership for Research in Interfacial and Materials Engineering (IPRIME) at the University of Minnesota. J.P. was supported by a research grant from the Young Scientists Fellowship of Hamburg University (Promotionsstipendium der Hamburgischen Nachwuchsförderung).

## APPENDIX

The following Figs. 14 present the complete data set of capillary thinning experiments. Figures 14(b) and 14(c) show the same data on two different time scales in order to capture the marked change in the relaxation time associated with changes in the polymer concentration  $c$  from  $5 \times 10^4$  ppm in DEP to 0.1 ppm in the viscous oligomer.

## References

- Amarouchene, Y., D. Bonn, J. Meunier, and H. Kellay, "Inhibition of the finite-time singularity during droplet fission of a polymeric fluid," *Phys. Rev. Lett.* **86**, 3558–3561 (2001).
- Amelar, S., C. E. Eastman, T. P. Lodge, and E. D. Vonmeerwall, "How good is the bead-spring model," *J. Non-Cryst. Solids* **131**, 551–555 (1991).
- Anna, S. L., and G. H. McKinley, "Elasto-capillary thinning and breakup of model elastic liquids," *J. Rheol.* **45**, 115–138 (2001).
- Anna, S. L., G. H. McKinley, D. A. Nguyen, T. Sridhar, S. J. Muller, J. Huang, and D. F. James, "An interlaboratory comparison of measurements from filament-stretching rheometers using common test fluids," *J. Rheol.* **45**, 83–114 (2001).
- Bazilevskii, A. V., V. M. Entov, M. M. Lerner, and A. N. Rozhkov, "Degradation of polymer solution filaments," *Vysokomol. Soedin., Ser. A Ser. B* **39**, 474–482 (1997).
- Bazilevskii, A. V., V. M. Entov, and A. N. Rozhkov, "Liquid filament microrheometer and some of its applications," *Third European Rheology Conference* 1990.
- Bazilevskii, A. V., V. M. Entov, and A. N. Rozhkov, "Breakup of an Oldroyd liquid bridge as a method for testing the rheological properties of polymer solutions," *Vysokomol. Soedin., Ser. A Ser. B* **43**, 716–726 (2001).
- Bird, R. B., O. Hassager, R. C. Armstrong, and C. F. Curtiss, *Dynamics of Polymeric Liquids—Kinetic Theory* (Wiley, New York, 1987), Vol. 2.
- Christanti, Y., and L. M. Walker, "Surface tension driven jet break up of strain-hardening polymer solutions," *J. Non-Newtonian Fluid Mech.* **100**, 9–26 (2001).
- Clasen, C., J. Eggers, M. A. Fontelos, J. Li, and G. H. McKinley, "The beads-on-string structure of viscoelastic threads," *J. Fluid Mech.* **556**, 283–308 (2006).
- Cooper-White, J. J., J. E. Fagan, V. Tirtaatmadja, D. R. Lester, and D. V. Boger, "Drop formation dynamics of constant low-viscosity, elastic fluids," *J. Non-Newtonian Fluid Mech.* **106**, 29–59 (2002).
- Doyle, P. S., E. S. G. Shaqfeh, and A. P. Gast, "Dynamic simulation of freely draining flexible polymers in steady linear flows," *J. Fluid Mech.* **334**, 251–291 (1997).
- Dunlap, P. N., and L. G. Leal, "Dilute polystyrene solutions in extensional flows—Birefringence and flow modification," *J. Non-Newtonian Fluid Mech.* **23**, 5–48 (1987).
- Eggers, J., "Nonlinear dynamics and breakup of free-surface flows," *Rev. Mod. Phys.* **69**, 865–929 (1997).
- Entov, V. M., and E. J. Hinch, "Effect of a spectrum of relaxation times on the capillary thinning of a filament of elastic liquid," *J. Non-Newtonian Fluid Mech.* **72**, 31–53 (1997).
- Entov, V. M., V. I. Kordonskil, and I. V. Prokhorov, "Rapid stretching of polymer solutions," *Sov. Phys. Dokl.* **33**, 628–630 (1988).
- Ferry, J. D., *Viscoelastic Properties of Polymers*, 3rd ed. (Wiley, New York, 1980).
- Ghosh, I., G. H. McKinley, R. A. Brown, and R. C. Armstrong, "Deficiencies of FENE dumbbell models in describing the rapid stretching of dilute polymer solutions," *J. Rheol.* **45**, 721–758 (2001).
- Graessley, W. W., "Polymer chain dimensions and the dependence of viscoelastic properties on the concentration, molecular weight and solvent power," *Polymer* **21**, 258–262 (1980).
- Gupta, R. K., D. A. Nguyen, and T. Sridhar, "Extensional viscosity of dilute polystyrene solutions: Effect of concentration and molecular weight," *Phys. Fluids* **12**, 1296–1318 (2000).
- Harrison, G. M., J. Remmelgas, and L. G. Leal, "The dynamics of ultradilute polymer solutions in transient flow: Comparison of dumbbell-based theory and experiment," *J. Rheol.* **42**, 1039–1058 (1998).
- Kalashnikov, V. N., "Shear-rate dependent viscosity of dilute polymer-solutions," *J. Rheol.* **38**, 1385–1403 (1994).
- Kolte, M. I., and P. Szabo, "Capillary thinning of polymeric filaments," *J. Rheol.* **43**, 609–625 (1999).
- Kulicke, W.-M., and C. Clasen, *Viscosimetry of Polymers and Polyelectrolytes* (Springer, Heidelberg, 2004).
- Larson, R. G., "The rheology of dilute solutions of flexible polymers: Progress and problems," *J. Rheol.* **49**, 1–70 (2005).
- Liang, R. F., and M. R. Mackley, "Rheological characterization of the time and strain dependence for polyisobutylene solutions," *J. Non-Newtonian Fluid Mech.* **52**, 387–405 (1994).

- Lindner, A., J. Vermant, and D. Bonn, "How to obtain the elongational viscosity of dilute polymer solutions?" *Physica A* **319**, 125–133 (2003).
- Mackay, M. E., and D. V. Boger, "An explanation of the rheological properties of Boger fluids," *J. Non-Newtonian Fluid Mech.* **22**, 235–243 (1987).
- Matta, J. E., and R. P. Tytus, "Liquid stretching using a falling cylinder," *J. Non-Newtonian Fluid Mech.* **35**, 215–229 (1990).
- McKinley, G. H., "Visco-elasto-capillary thinning and breakup of complex fluids," in: *Annual Rheology Reviews*, edited by D. M. Binding and K. Walters (British Society of Rheology, Aberystwyth, 2005), pp. 1–48.
- McKinley, G. H., and T. Sridhar, "Filament-stretching rheometry of complex fluids," *Annu. Rev. Fluid Mech.* **34**, 375–415 (2002).
- McKinley, G. H., and A. Tripathi, "How to extract the Newtonian viscosity from capillary breakup measurements in a filament rheometer," *J. Rheol.* **44**, 653–670 (2000).
- Nguyen, T. Q., and H. H. Kausch, *Flexible Polymer Chains in Elongational Flow: Theory & Experiment* (Springer-Verlag, Berlin, 1999).
- Öttinger, H. C., *Stochastic Processes in Polymeric Liquids* (Springer Verlag, Berlin, 1996).
- Papageorgiou, D. T., "On the breakup of viscous liquid threads," *Phys. Fluids* **7**, 1529–1544 (1995).
- Plog, J. P., W. M. Kulicke, and C. Clasen, "Influence of the molar mass distribution on the elongational behaviour of polymer solutions in capillary breakup," *Appl. Rheol.* **15**, 28–37 (2005).
- Prabhakar, R., J. R. Prakash, and T. Sridhar, "Effect of configuration-dependent intramolecular hydrodynamic interaction on elasto-capillary thinning and break-up filaments of dilute polymer solutions," *J. Rheol.* (to be published).
- Rodd, L., T. Scott, J. Cooper-White, and G. H. McKinley, "Capillary break-up rheometry of low-viscosity elastic fluids," *Appl. Rheol.* **15**, 12–27 (2005).
- Rubinstein, M., and R. H. Colby, *Polymer Physics*, (Oxford University Press, New York, 2003).
- Schroeder, C. M., H. P. Babcock, E. S. G. Shaqfeh, and S. Chu, "Observation of polymer conformation hysteresis in extensional flow," *Science* **301**, 1515–1519 (2003).
- Slobozhanin, L. A., and J. M. Perales, "Stability of liquid bridges between equal disks in an axial gravity-field," *Phys. Fluids A* **5**, 1305–1314 (1993).
- Solomon, M. J., and S. J. Muller, "Study of mixed solvent quality in a polystyrene dioctyl phthalate polystyrene system," *J. Polym. Sci., Part B: Polym. Phys.* **34**, 181–192 (1996).
- Sridhar, T., V. Tirtaatmadja, D. A. Nguyen, and R. K. Gupta, "Measurement of extensional viscosity of polymer solutions," *J. Non-Newtonian Fluid Mech.* **40**, 271–280 (1991).
- Stelter, M., and G. Brenn, "Validation and application of a novel elongational device for polymer solutions," *J. Rheol.* **44**, 595–616 (2000).
- Stelter, M., G. Brenn, A. L. Yarin, R. P. Singh, and F. Durst, "Investigation of the elongational behavior of polymer solutions by means of an elongational rheometer," *J. Rheol.* **46**, 507–527 (2002).
- Stoltz, C., J. J. dePablo, and M. D. Graham, "Concentration dependence of shear and extensional rheology of polymer solutions: Brownian dynamics simulations," *J. Rheol.* **50**, 137–167 (2006).
- Tam, K. C., and C. Tiu, "Improved correlation for shear-dependent viscosity of polyelectrolyte solutions," *J. Non-Newtonian Fluid Mech.* **46**, 275–288 (1993).
- Tirtaatmadja, V., G. H. McKinley, and J. J. Cooper-White, "Drop formation and breakup of low viscosity elastic fluids: Effects of molecular weight and concentration," *Phys. Fluids* **18**, 043101 (2006).
- Yao, M. W., S. H. Spiegelberg, and G. H. McKinley, "Dynamics of weakly strain-hardening fluids in filament stretching devices," *J. Non-Newtonian Fluid Mech.* **89**, 1–43 (2000).